การเตรียมคาร์บอนดอตเติมหมู่ฟังก์ชันด้วยกรดโบโรนิกสำหรับการตรวจวัดกลูโคสผ่านปฏิกิริยาเร่งด้วยเอนไซม์กลูโคสออกซิเดส

นางสาวอังคณา ขจรวงศ์วัฒนา

วิทยานิพนธ์นี้เป็นส่วนหนึ่งของการศึกษาตามหลักสูตรปริญญาวิทยาศาสตรมหาบัณฑิต
สาขาวิชาเคมี ภาควิชาเคมี
คณะวิทยาศาสตร์ จุฬาลงกรณ์มหาวิทยาลัย
ปีการศึกษา 2559

PREPARATION OF BORONIC ACID FUNCTIONALIZED CARBON DOTS FOR GLUCOSE DETECTION VIA ENZYMATIC REACTION OF GLUCOSE OXIDASE

Miss Angkhana Khachonwongwattana

A Thesis Submitted in Partial Fulfillment of the Requirements
for the Degree of Master of Science Program in Chemistry
Department of Chemistry
Faculty of Science
Chulalongkorn University
Academic Year 2016

Thesis Title	PREPARATION OF BORONIC ACID FUNCTIONALIZED CARBON DOTS FOR GLUCOSE DETECTION VIA ENZYMATIC REACTION OF GLUCOSE OXIDASE
By	Miss Angkhana Khachonwongwattana
Field of Study	Chemistry
Thesis Advisor	Assistant Professor Boosayarat Tomapatanaget, Ph.D.
Thesis Co-Advisor	Wipark Anutrasakda, Ph.D.

Accepted by the Faculty of Science, Chulalongkorn University in Partial Fulfillment of the Requirements for the Master's Degree

.....Dean of the Faculty of Science
(Associate Professor Polkit Sangvanich, Ph.D.)

THESIS COMMITTEE

.....Chairman
(Associate Professor Vudhichai Parasuk, Ph.D.)

.....Thesis Advisor
(Assistant Professor Boosayarat Tomapatanaget, Ph.D.)

.....Thesis Co-Advisor
(Wipark Anutrasakda, Ph.D.)

.....Examiner
(Assistant Professor Thanit Praneenararat, Ph.D.)

.....External Examiner
(Gamolwan Tumcharern, Ph.D.)

อังคณา ขจรวงศ์วัฒนา : การเตรียมคาร์บอนดอตเติมหมู่ฟังก์ชันด้วยกรดโบโรนิกสำหรับการตรวจวัดกลูโคสผ่านปฏิกิริยาเร่งด้วยเอนไซม์กลูโคสออกซิเดส (PREPARATION OF BORONIC ACID FUNCTIONALIZED CARBON DOTS FOR GLUCOSE DETECTION VIA ENZYMATIC REACTION OF GLUCOSE OXIDASE) อ.ที่ปรึกษาวิทยานิพนธ์หลัก: ผศ. ดร.บุษยรัตน์ ธรรมพัฒนกิจ, อ.ที่ปรึกษาวิทยานิพนธ์ร่วม: ดร.วิภาค อนุตรศักดา, 80 หน้า.

ในงานวิจัยนี้คณะผู้วิจัยได้ทำการศึกษาอนุภาคคาร์บอนระดับนาโนเมตร ซึ่งสังเคราะห์ผ่านกระบวนการไฮโดรเทอร์มอลคาร์บอไนเซชันเพียงขั้นตอนเดียวโดยใช้ 3 ไอโซเมอร์ของกรดอะมิโนฟีนิลโบโรนิกเป็นสารตั้งต้นเพื่อเตรียมอนุภาคคาร์บอนระดับนาโนเมตรที่มีชื่อว่า *o*-BCDs, *m*-BCDs และ *p*-BCDs การศึกษาลักษณะโครงสร้างภายนอกและสมบัติของโครงสร้างโมเลกุลโดยใช้เทคนิคอินฟราเรดสเปกโทรสโกปี (FT-IR) กล้องจุลทรรศน์อิเล็กตรอนแบบส่องผ่าน (TEM) กล้องจุลทรรศน์แรงอะตอม (AFM) สเปคโตรสโคปีของอนุภาคอิเล็กตรอนที่ถูกปลดปล่อยด้วยรังสีเอกซ์ (XPS) และโบรอน-นิวเคลียร์แมกเนติกเรโซแนนซ์สเปคโตรสโคปี (^{11}B-NMR spectroscopy) พบว่าคาร์บอนดอตที่สังเคราะห์ได้มีลักษณะเป็นแผ่นชั้นเดียวของกราฟีนที่มีรูปร่างค่อนข้างกลมและมีความเป็นรูปแบบเดียวกันต่ำ โครงสร้างองค์ประกอบของ *o*-BCDs และ *p*-BCDs มีความคล้ายคลึงกันซึ่งแตกต่างจาก *m*-BCDs โครงสร้างที่ต่างกันนำไปสู่คุณสมบัติที่แตกต่างกัน โดยอนุภาคทั้งสามมีการคายแสงฟลูออเรสเซนต์ที่ความยาวคลื่นแตกต่างกันที่ 345, 375 และ 343 นาโนเมตร อีกทั้งยังมีค่าการเปล่งแสงเชิงควอนตัมเท่ากับ 3.02%, 17.26% และ 3.30% ตามลำดับ นอกจากนี้อนุภาคคาร์บอนระดับนาโนเมตรแต่ละชนิดถูกนำไปพัฒนาเป็นตัวตรวจวัดน้ำตาลกลูโคสด้วยเทคนิคทางฟลูออเรสเซนต์โดยอาศัยหลักการตรวจวัดไฮโดรเจนเปอร์ออกไซด์ (H_2O_2) ที่ผลิตมาจากปฏิกิริยาทางเอนไซม์ของกลูโคสออกซิเดส (GOx) และกลูโคส จากผลการทดสอบด้วยเทคนิคฟลูออเรสเซนซ์สเปกโทรสโกปีพบการลดลงของความเข้มของการคายพลังงาน (fluorescence intensity) ขึ้นอยู่กับความเข้มข้นของไฮโดรเจนเปอร์ออกไซด์ที่ผลิตมาจากปฏิกิริยาทางเอนไซม์ซึ่งสัมพันธ์กับปริมาณของกลูโคสที่เติมเข้าไป เป็นที่น่าสนใจว่า *m*-BCDs เป็นอนุภาคเดียวที่สามารถตรวจวัดน้ำตาลกลูโคสได้ด้วยด้วยค่าขีดจำกัดการตรวจวัดเท่ากับ 0.857 มิลลิโมลาร์ (mM) และขีดจำกัดการวัดเชิงปริมาณเท่ากับ 2.858 mM ในขณะที่ *o*-BCDs และ *p*-BCDs สามารถตรวจวัดได้เพียงไฮโดรเจนเปอร์ออกไซด์ที่ใส่เข้าไปทำปฏิกิริยา แต่ไม่สามารถตรวจวัดไฮโดรเจนเปอร์ออกไซด์ที่ผลิตมาจากปฏิกิริยาทางเอนไซม์ได้

ภาควิชา	เคมี	ลายมือชื่อนิสิต	.....
สาขาวิชา	เคมี	ลายมือชื่อ อ.ที่ปรึกษาหลัก	.....
ปีการศึกษา	2559	ลายมือชื่อ อ.ที่ปรึกษาร่วม	.....

5772214923 : MAJOR CHEMISTRY
KEYWORDS: ENZYMATIC REACTION / CARBON DOTS, HYDROGEN PEROXIDE DETECTION, GLUCOSE DETECTION,

ANGKHANA KHACHONWONGWATTANA: PREPARATION OF BORONIC ACID FUNCTIONALIZED CARBON DOTS FOR GLUCOSE DETECTION VIA ENZYMATIC REACTION OF GLUCOSE OXIDASE. ADVISOR: ASST. PROF. BOOSAYARAT TOMAPATANAGET, Ph.D., CO-ADVISOR: WIPARK ANUTRASAKDA, Ph.D., 80 pp.

In this study, novel BCDs materials were synthesized by one step hydrothermal carbonization using three isomers (ortho-, meta- and para-) of aminophenylboronic acid as a precursor for preparing the carbon dots, namely, *o*-BCDs, *m*-BCDs and *p*-BCDs. The morphology and structural properties of these BCDs were investigated by FT-IR, AFM, TEM, XPS techniques and ^{11}B-NMR spectroscopy. From TEM and AFM image, the BCDs are single layer of graphene sheet and the fairly uniform of spherical quasi circular sheet. From XPS techniques and ^{11}B-NMR spectroscopy, *o*-BCDs and *p*-BCDs have the similar component structures which is different from *m*-BCDs. The different structure leaded to the different emission bands of *o*-, *m*- and *p*-BCDs at 345 nm, 375 nm and 343 nm with quantum yield of 3.02%, 17.26% and 3.30%, respectively. Each BCDs material was applied as a fluorescent probe for H_2O_2 and glucose sensing application. For enzymatic glucose biosensor, the fluorescence quenching of BCDs depended on the concentration of H_2O_2 which was generated from enzymatic reaction by glucose and GOx. Interestingly, the *m*-BCDs served as an excellent fluorescent probe for glucose detection via enzymatic reaction with LOD of 0.857 mM and LOQ of 2.858 mM whereas *o*-BCDs and *p*-BCDs can detect only added H_2O_2 but H_2O_2 generated from enzymatic reaction by glucose and GOx cannot be determined.

Department:	Chemistry	Student's Signature	.....
Field of Study:	Chemistry	Advisor's Signature	.....
Academic Year:	2016	Co-Advisor's Signature	.....

ACKNOWLEDGEMENTS

I would like to thank all the following people for their advices, assistances, and supports during my study:

Firstly, I am deeply obliged to my thesis advisor Asst. Prof. Dr. Boosayarat Tomapatanaget for giving me the great opportunity to do the research, and suggestions, supports, inspiration for this research as well as introducing the new knowledge about nanomaterials and enzymatic reaction.

I would like to thank my co-advisor Dr. Wipark Anutrasakda for assistances and encouragements during my work as well as my committees, Assoc. Prof. Dr. Vudhichai Parasuk, Asst. Prof. Dr. Thanit Praneenararat and Dr. Gamolwan Tumcharern for their valuable suggestions and comments.

Moreover, I am grateful to Dr. Gamolwan Tumcharern for assistance in morphology studies by using the transmission electron microscopy (TEM) as well as all the members in the Supramolecular Chemistry Research Unit (SCRU) for their friendships, encouragements, suggestions and assistances.

Additionally, I would like to acknowledge Department of Chemistry, Chulalongkorn University and the Ratchadapisek Sompoch Endowment Fund (2016), Chulalongkorn University (CU-59-020-FW) for financial supports.

Finally, I would like to give a special thanks to my close friends and my family, especially my grandmother for their huge loves, cares, kindnesses, encouragements and for always standing by my side no matter what happens.

CONTENTS

Page

Page

Page

LIST OF FIGURES

LIST OF SCHEMES

LIST OF TABLES

LIST OF ABBREVIATIONS AND SYMBOLS

AFM	Atomic force microscopy
^{11}B-NMR	Boron nuclear magnetic resonance
BCDs	Boron doped carbon dots
BGQDs	Boron-doped graphene quantum dots
CDs	Carbon dots
CQDs	Carbon quantum dots
δ	Chemical Shift
eV	Electron volt
equi.	Equivalent
GQDs	Graphene quantum dots
g	Gram
µg	Microgram
h	Hour
H_2O_2	Hydrogen peroxide
min	Minute
Hz	Hertz
µL	Microliter
mmol	Millimole

mL	Milliliter
nm	Nanometer
m-	Meta
M	Molar
mM	Milimolar
o-	Ortho
p-	Para
PDs	Polymer dots
TEM	Transmission Electron Microscopy
FT-IR	Fourier transform infrared spectroscopy
XPS	X-ray photoelectron spectroscopy

CHAPTER I

INTRODUCTION AND LITERATURE REVIEWS

1.1 Diabetes mellitus

Diabetes mellitus is one of the biggest public health threats of clinical disease. Recently, over 200 million people have suffered from this disease and will reach to 300 million people in 2030. The patients need to constantly monitor their blood glucose levels. This is very important in following their symptoms because high glucose level in blood can cause serious problems with body function such as eyes, feet, kidneys, heart, and nerve [1, 2].

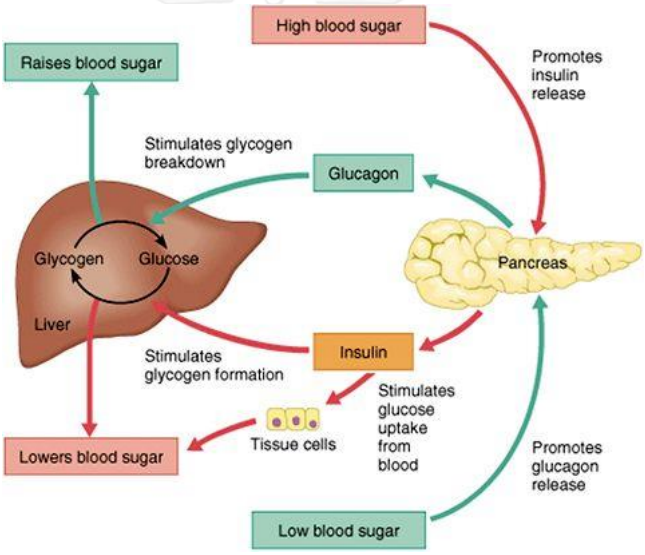

Figure 1.1 Glucose metabolic pathway [3].

High glucose levels in blood lead to release insulin by pancreases. The hormone can stimulate glucose uptaking from blood stream and transforming the glucose to glycogen. The glycogen is collected in liver and released in case of low blood glucose levels. Thus, insulin can control amount of glucose in blood in suitable level. For diagnosis of diabetes mellitus, the blood glucose level after fasting for 8 hours is higher than 126 mg/dL or 7.0 mmol/L.

In the development of sensor systems for glucose detection, concentration of glucose can be determined via 2 methods; non-enzymatic methods and enzymatic methods. The case of non-enzymatic methods, this method has been attended because of simple and reproducibility. However, it is poor stability and lack of selective recognition units in some case. In the development of non-enzymatic glucose sensor, boronic acid derivatives being an essential reactive site in monosaccharides detection that boronic ester is formed as shown in equation 1.

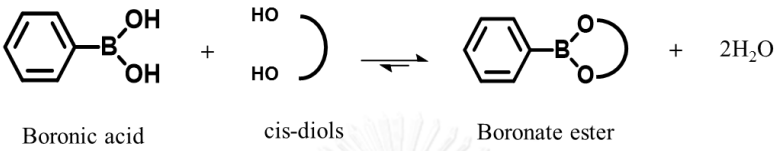

.....(1)

For example, Hua and co-workers used GQDs with a boronic acid substituted bipyridinium salt (BBV) as a label-free fluorescence assay for glucose detection. The mechanism of this sensor as show in scheme 1.1.

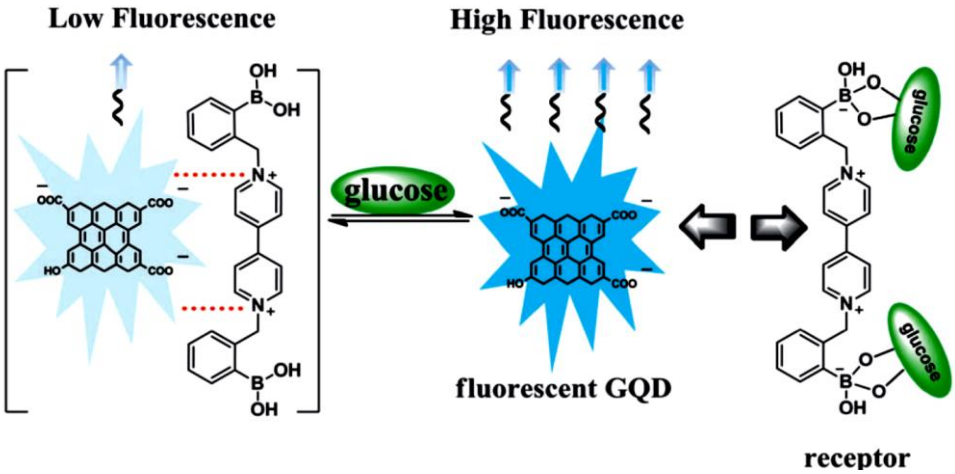

Scheme 1. 1 Proposed glucose- sensing mechanism based on BBV receptor and fluorescent GQDs [4].

This research found that not only glucose can be detected by this system but also other monosaccharides such as galactose and fructose can be detected as well. Thus, this work we have focused on enzymatic method because this method is more specific to analyte than non-enzymatic method.

1.2 Enzymatic biosensor

1.2.1 Definition of biosensors

A biosensor is an analytical device for bioanalyte detection which is constructed by the high affinity and high specificity bio-recognition molecules such as enzymes, antibodies, aptamers, DNAzymes and whole cells [5-9] for the interaction with the targets (Scheme 1.2). The working principal of these biosensors based on cooperation between transducer and biological component. The interaction of the analytes with bio-recognition molecules is translated to signal. Owing to the fact that these biosensors supply highly sensitive, and high-frequency monitoring without any time-consuming concentration of sample and former sample pre-treatment steps, biosensor applications have been widely used in the areas of environmental monitoring, food safety, drug development, biomedical research, and diagnosis[10-14].

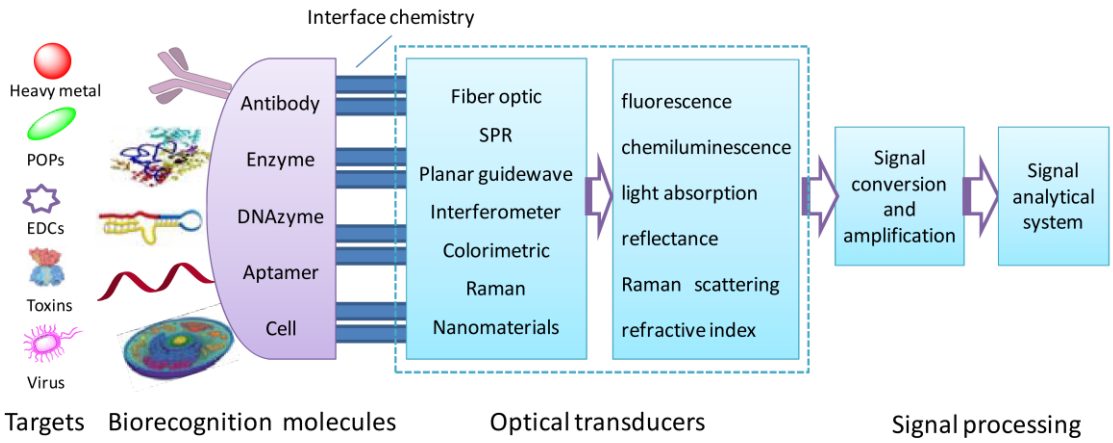

Scheme 1.2 Schematic of an optical biosensor [10].

1.2.2 Biorecognition molecules

The fundamental and key feature of a biosensor is the construction of the bio-recognition element for the interaction with the targets. Functional biomaterials upon the high affinity and high specificity include antibodies, enzymes, functional oligonucleotides and whole cells [8-10]. In several research studies about glucose detection via enzymatic reaction suggested that the boronic acid is a reactive site to

react with H_2O_2. In general, H_2O_2 and hydroxyl group based on molecular sensor are provided from the reaction as shown in equation 2 [15].

$$R\text{-}B(OR)_2 + H_2O_2 \longrightarrow R\text{-}OH + B(OH)(OR_2) \quad \text{.....(2)}$$

1.2.3 Enzymatic glucose biosensor

In a past decade, enzyme-based biosensors have been particularly interesting area of biosensor because of their specificity to target. Due to the fact that glucose cannot be directly detected under highly effective specific detection, the determination of H_2O_2, which is an end product from many enzymatic reactions including glucose oxidase (GOx), plays a crucial role for screening and diagnosis.

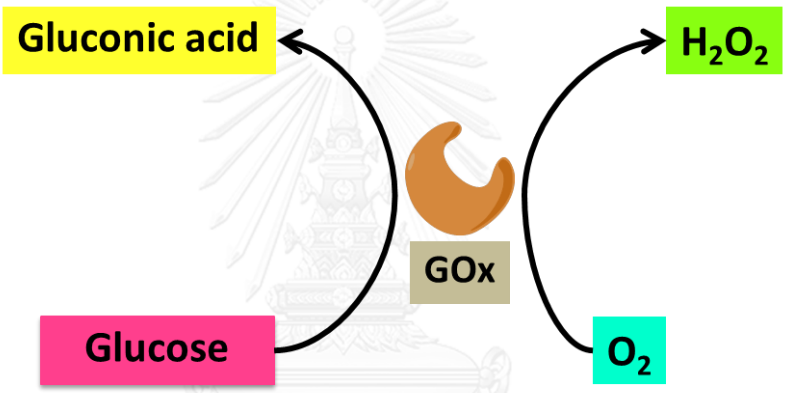

Scheme 1.3 The concept of glucose biosensor through enzymatic mechanism.

For the enzymatic reaction, glucose reacts with GOx in the presence of O_2. Then, the oxidation of glucose to gluconic acid and H_2O_2 has been catalyzed. The mechanism is shown in scheme 1.3.

In 2012, Wannajuk and co-workers studied the application of boronic-based fluorescence sensor for selective detection of glucose. They developed the new boronic-based anthraquinone to determine glucose under the basic knowledge of GOx enzymatic reaction as illustrated in scheme 1.4 [16].

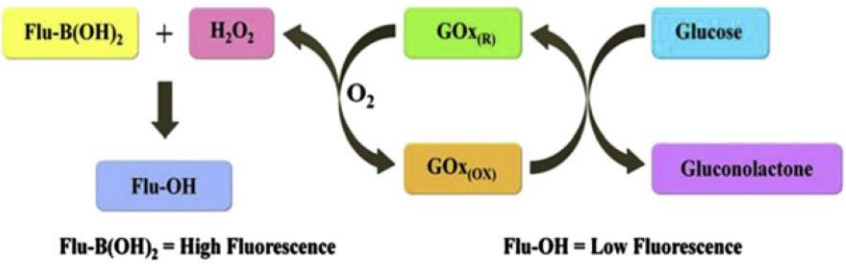

Scheme 1.4 The GOx enzymatic mechanism for glucose detection using boronic-based fluorescence sensors [16].

This research has reported the successful fluorescence probe to detect glucose through enzymatic reaction in the range of concentration 0.08-0.42 mM with the limit of detection of glucose at 0.011 mM.

For another example of boronic acid based on fluorophore applied in H_2O_2 detection, Alexander and co-workers demonstrated the boronate oxidation as a bioorthogonal reaction approach to study the chemistry of hydrogen peroxide in living systems [17]. The monoboronate bearing fluorophores has offered to be one of the effective chemical tools for monitoring H_2O_2 in live-cell microscopy experiments. The methods for reaction-based trapping inside cells can be useful for interrogating the H_2O_2 production, and H_2O_2 in other systems such as growth factor signaling, immune response, and stem cell (Figure 1.2).

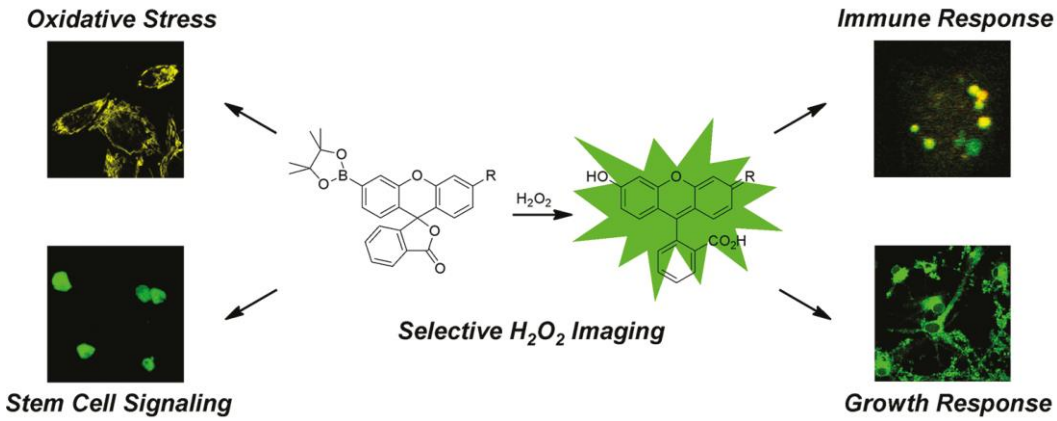

Figure 1.2 Bioluminescence selective H_2O_2 imaging [17].

Moreover, many research in glucose detection – both non-enzymatic methods and enzymatic methods – have focused on using nanomaterial as sensors in diabetes diagnosis especially carbon dots (CDs) in a past several years.

1.3 Carbon dots (CDs)

Carbon dots (CDs) is a term of fluorescent carbon nanomaterials composing of sp^2-sp^3 carbon and oxygen/nitrogen-based group or polymeric aggregations in their structure. The materials own at least one dimension with a size less than 10 nm. The fluorescence property of CDs bases on their unique properties such as size, edge and surface chemistry. In the past decade, CDs have attracted interest due to their low cost, low toxicity, biocompatibility and easy to functionalize. Normally, CDs can be categorized into 3 types [3]: Graphene quantum dots (GQDs), Carbon nanodots (CNDs), and Polymer dots (PDs). Their classification is considered by structure and morphology of them as shown in figure 1.3.

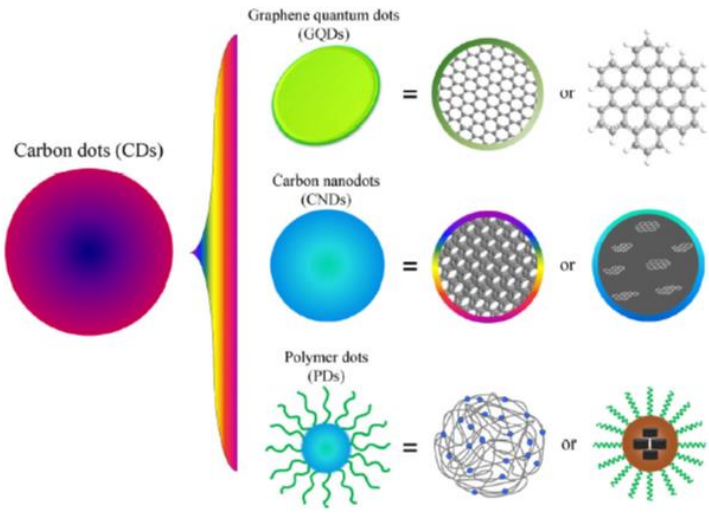

Figure 1.3 Three types of fluorescent carbon dots: graphene quantum dots (GQDs), carbon nanodots (CNDs), and polymer dots (PDs) [3].

- Graphene quantum dots (GQDs) are a type of CDs, consisting of one or a few layers of graphene sheet with diameter less than 10 nm. The edges may be surrounded with chemical group. The photoluminescence (PL) properties of GQDs based on several effects such as the synthetic process, doping atom and edge type. Firstly, the different synthetic processes also provide different size of particles resulting in various PL response. And the different doping atom in GQDs also provides different quantum yield (QYs) of them. Finally, edge types of the particles, including zigzag-edge or armchair edge, seem to play crucial role in the PL mechanism.

- Carbon nanodots (CNDs) have a much more comprehensive meaning comparing with GQDs. CNDs can be classified into two groups namely carbon nanoparticles (CNP) and carbon quantum dots (CQDs). The classification is considered by structure and morphology of them. Carbon nanoparticles are always spherical and have no a crystal lattice, while CQDs have an obvious crystal lattice. The PL properties of CNDs are similar to those of GQDs but the different structure results in different PL properties. Not only structure of CNDs can affect to PL properties but also the different functional group on CNDs will give the different PL properties. Since different functional group leads to different energy levels [18]. In addition, the surface doped with

nanoscale semiconductors and the organic functionalized fluorophore can improve fluorescence emission namely QYs of CNDs [19].

- Polymer dots (PDs) can be classified into 2 types; non-conjugated PDs and conjugated PDs. PDs are constructed photoluminescence depending on type of PDs. Owning to more rigidity of PDs structure, non-radiative decay has been decreased resulting in an increase of fluorescence signal and high stability of the particles [3].

1.3.1 Synthetic method of carbon dots

There are many approaches to fabricate high quality CDs. The most general approaches for synthesis of C-dots can be classified into 2 methods including "top-down" and "bottom-up" [20] as shown in figure 1.4

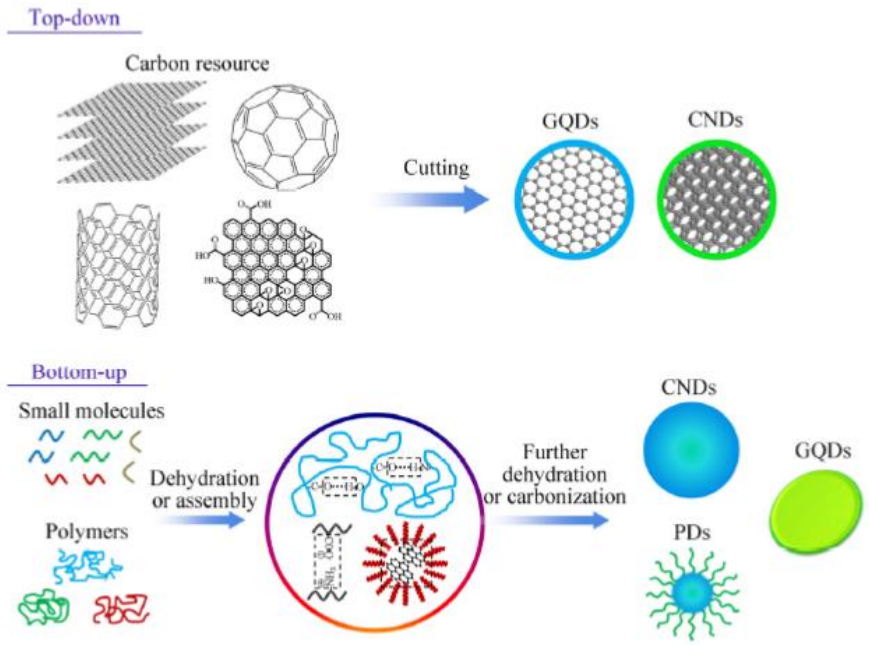

Figure 1.4 The main processes to synthesize CDs: "Top-down" cutting from various sp^2-carbon materials and "bottom-up" synthesis from small molecules [15].

1.3.1.1 Top-Down method

Top-Down method involves the process of cleaving or breaking down of bulk carbon materials such as carbon fibers [21], carbon nanotube [22], graphene sheet [23] or carbon black [24], via chemical, electrochemical, or physical approaches to small

pieces of carbon dots which is known as GQDs, CQDs, or CNDs. The surfaces of the small products are modified by oxidizing agents such as concentrated H_2SO_4 or HNO_3. However, the use of this method is limited by the need of sophisticated equipment.

1.3.1.2 Bottom-Up method

Bottom-Up method is the process which constructs carbon dots from small organic molecules or polymers by dehydration or assembly (carbonization) processes via pyrolysis, hydrothermal, solvothermal, or microwave methods [25, 26]. The applied molecules which contain –OH, -NH_2, -COOH, and -CO groups can undergo dehydration and further carbonization to form CDs. These methods are productive route to produce CDs on a large scale, as well as are simple, cost-effective, scalable and allowance of natural inheritance of heteroatoms from the precursors.

CDs are alternative nanomaterials which can be used as fluorescence probe to improve both non-enzymatic and enzymatic glucose determination.

In 2013, Zheng and coworkers reported graphene dots (GDs) as a highly-efficient peroxidase-like catalytic activity for biosensing application. In this research, glucose and the reduced glutathione (GSH) were investigated by monitoring the amount of H_2O_2 in those systems. In detection of glucose, H_2O_2 generated by enzymatic reaction of GOx activates GDs to be a reducing agent, and then 3,3,5,5-tetramethylbenzidine (TMB) was oxidized by the GDs to produce a blue product of oxTMB (The mechanism as shown in figure 1.5). Therefore, the amount of H_2O_2 was investigated by detection of oxTMB which shows absorbance change at 652 nm. Owing to its high catalytic activity, the GDs-based system shows the low detection limit of H_2O_2 being 10 mM, while limit of detection of glucose and GSH was 0.5 μM. Hence, glucose and GSH can be monitored effectively by the GDs. Therefore, this system was expected to be used in clinical care and biotechnology.

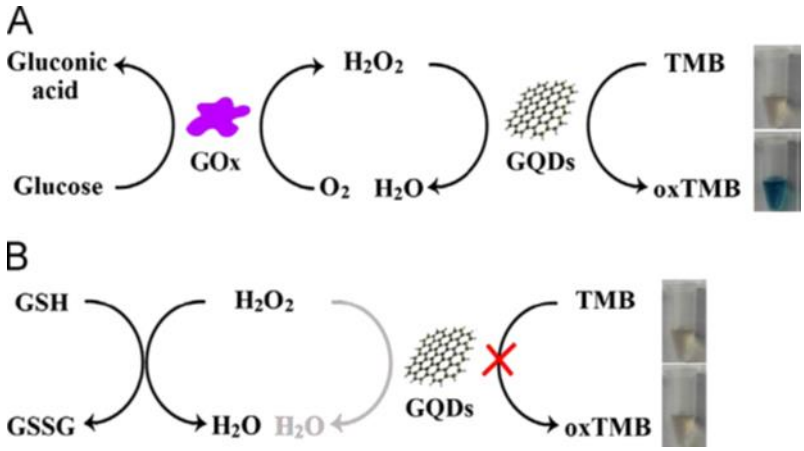

Figure 1.5 Schematic illustration of highly-efficient peroxidase-like activity of graphene dots (GDs) for the detection of H_2O_2, glucose and reduced glutathione (GSH) [27].

However, compared to inorganic semiconductor quantum dots and organic dyes, CDs are limited in fluorescent determination because of their low quantum yield. To overcome this drawback, surface modification with polymer or small organic molecules was developed to achieve high specificity and sensitive fluorescent efficiency [27-29]. Several fabrications of CD-based sensing systems have been reported.

A new class of N-doped quantum dots with unique properties for advanced device was investigated in 2011 [30]. Researchers developed a simple effective electrochemical strategy for generating N-doped GQDs with oxygen atom rich functional groups, which showed unique optoelectronic features compared to the N-free GQDs counterparts. The sizes of newly produced N-GQDs (around 2–5 nm) are much smaller than those of the N-free GQDs counterparts prepared by hydrothermal method (∼10 nm). The N-GQDs emitted blue luminescence and possessed an electrocatalytic activity (Figure 1.6). Moreover, the superior luminescence characteristic of N-GQDs offered the promising sensitivity for biomedical imaging and other optoelectronic applications.

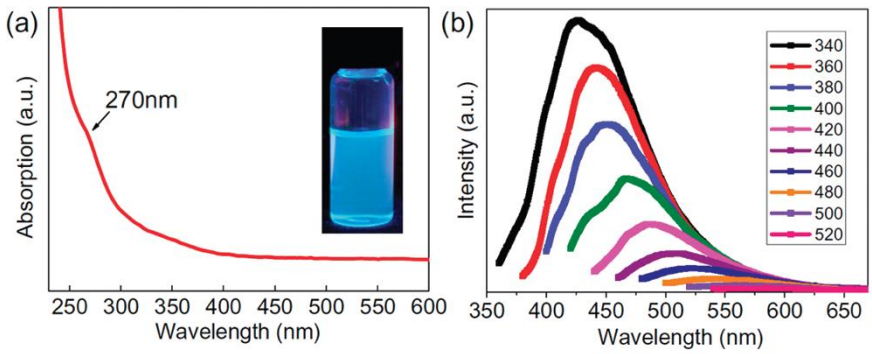

Figure 1.6 (a) UV-vis absorption and (b) PL spectra of N-GQDs in water. The inset in (a) is a photograph of the N-GQDs solution in water under 365 nm UV irradiation [30].

In 2013, Qu and co-workers revealed a boronic acid functionalized graphene quantum dot as a selective and sensitive fluorescent probe for glucose determination in microlysate [31]. GQDs were modified with aminobenzeneboronic acid (APBA) to form the APBA-GQDs that have higher quantum yield than GQDs (Scheme 1.5). The results showed that the quantum yield of the APBA-GQDs was 49.7%, which was 17.2 folds higher than that of original GQDs. The average size of the APBA-GQDs was 2.6 nm and the average thickness was 1. 5 nm (about 2 layers of graphene sheets). The aggregation of the glucose bound APBA-GQDs resulted in fluorescence quenching (Figure 1.7). The basal glucose concentration in the striatum of rat was calculated to be 0.42 ± 0.05 mM, demonstrating that this molecule has successfully been applied to monitor glucose in vivo.

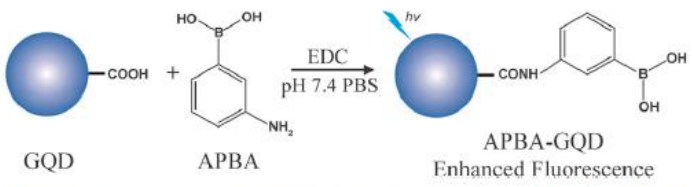

Scheme 1.5 Schematic representation of the functionalization of GQDs with APBA [31].

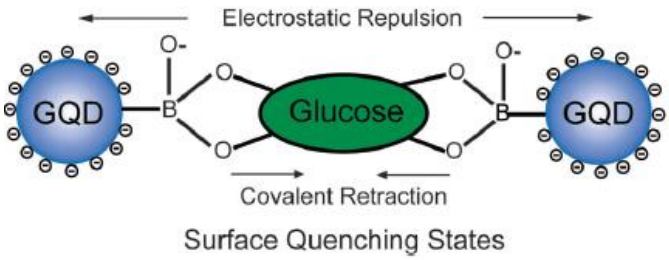

Figure 1.7 Proposed mechanism of surface quenching stated (SQS) for glucose sensing [31].

In principle, nanochemosensors were fabricated by at least two steps including synthesis of nanoparticle (NP) and particle surface functionalization for the introduction of recognition sites [32]. However, there has been a problem from aggregation of the reacted NPs. To overcome this drawback, in 2014, Shan and co-workers studied a new easy way to synthesize B-doped carbon quantum dots (BCQDs) by a facile one-pot route and the result suggested that the doping of boron into CQDs can largely enhance the fluorescence intensity (Scheme 1.6) [33]. The limit of detection for glucose by BCQDs was 8 μM, which is lower than that of other CQD-based fluorescence sensors.

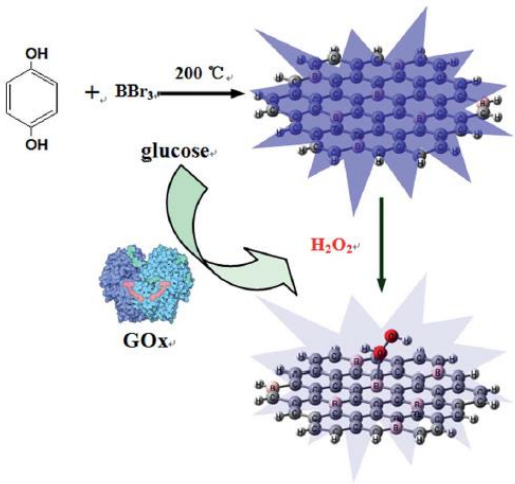

Scheme 1.6 Schematic representation of synthesis of BCQDs and glucose-sensing mechanisms based on BCQDs and H_2O_2 [33].

In the same year, Zhang and co-workers reported a novel hydrothermal approach for cutting boron-doped graphene (BG) to generate boron-doped graphene quantum dots (BGQDs) [34]. The BGQDs were used as a new photoluminescence (PL)

probe for labeling free glucose sensing. Based on the conceptually new mechanism of GQDs sensing, the PL of BGQDs in the presence of glucose was enhanced by the restriction of the intramolecular rotations activated by the particular BGQDs-glucose interactions (Scheme 1.7).

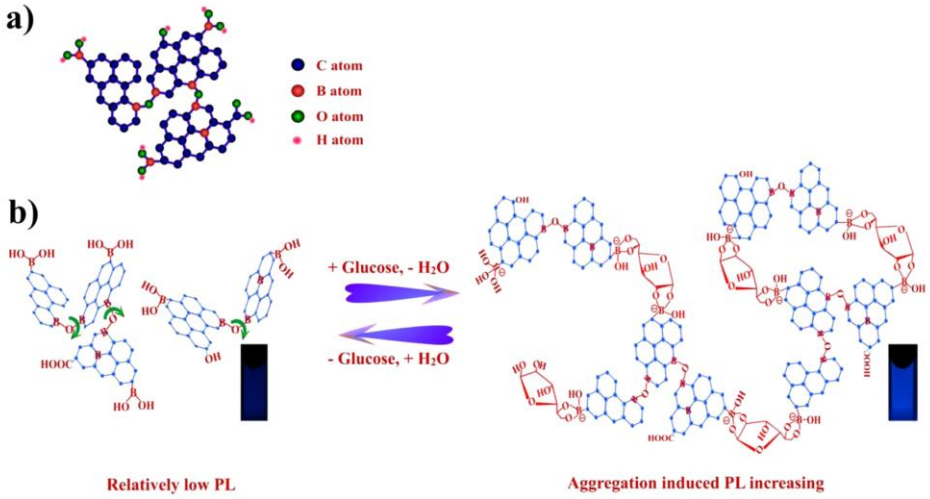

Scheme 1.7 a) Schematic representation of the boron-doped graphene quantum dots (BGQDs). b) Proposed "aggregation-induced PL increasing" mechanism for the glucose-specific sensing by BGQDs [34].

Another inspiration for our work has been reported by Jiang and co-worker. They prepared carbon dots (CDs) by three isomers of phenylenediamine (ortho, meta and para) via solvothermal method for used in cellular imaging. The as-prepared CDs which is ***o***-CDs, ***m***-CDs and ***p***-CDs provide strong green, blue and red, respectively, under single excitation wavelength of 365 nm. Moreover, these CDs show up-conversion photoluminescence; These CDs thus, can be applied in cellular imaging (Figure 1.8).

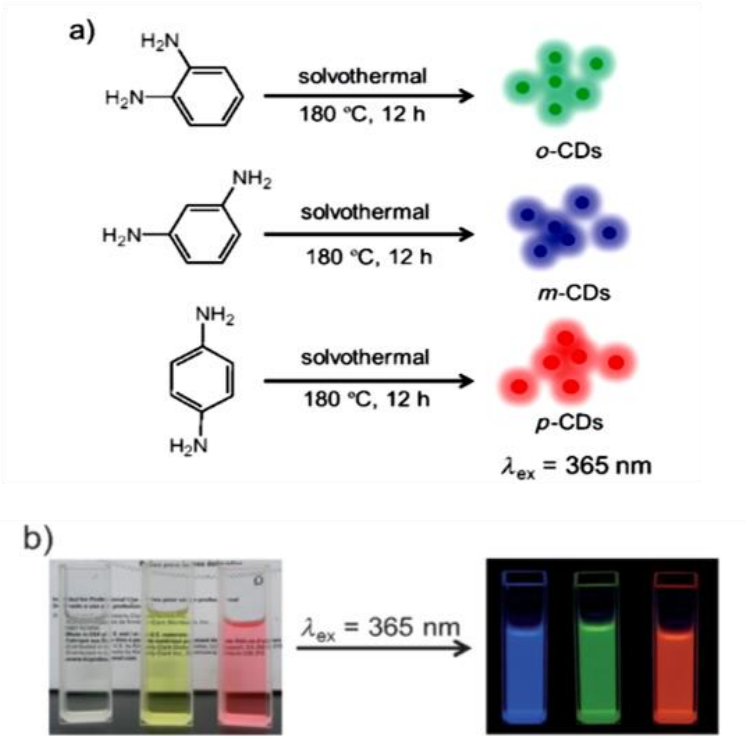

Figure 1.8 a) Preparation of the RGB PL CDs from three different phenylenediamine isomers (i.e., *o*PD, *m*PD and *p*PD). b) Photographs of ***m***-CDs, ***o***-CDs, and ***p***-CDs dispersed in ethanol in daylight (left), and under λ_{ex} =365 nm UV irradiation (right) [35].

Taking on aboard of literature reviews, they alert us the idea to develop glucose and H_2O_2 sensing in biological and environmental systems under fluorescence technique. The high selectivity and low detection limit for target analysts are required. In this research, we have focused on design and synthesis of CDs grafted with nitrogen atom and specific binding site of boronic acid that can interact with glucose and H_2O_2. We are interested in preparation of different types of CDs materials from three isomers of aminophenylboronic acid namely ***o***-, ***m***- and ***p***-aminophenylboronic acid as the starting material which contain boronic acid as a reactive site for reacting with glucose and amino group as an electron donating group leading to longer emission band (red-shift). Moreover, enzymatic reaction of GOx was also applied in glucose sensing. The GOx enzyme specifically reacting with glucose results in H_2O_2 generating. In order to determine the amount of glucose, the generated H_2O_2 from GOx and glucose reaction is indirect analyte that is proportional to the amount of glucose. This expectation may

provide a new fluorescence sensor based on **BCDs** for detection of glucose in sensing approach.

.

CHAPTER II

EXPERIMENTAL

2.1 General Procedure

2.1.1 Analytical measurements

^{11}B nuclear magnetic resonance (NMR) spectra were recorded by a Bruker-500 (500 MHz) spectrometer at room temperature. The chemical shifts were reported in part per million (ppm) relative to a residual deuterated CD_3OD and D_2O signal. Transmission electron microscopy (TEM) was performed on a JEOL JEM 2010 with a field emission gun operated at 200 kV. The TEM micrographs were used to examine the morphology of CDs by counting approximately 20 particles (ImageJ software, Scion Corporation). Atomic force microscope (AFM) was performed on veeco MultiMode™ system with NanoScope Analysis Version 1.40 software. IR spectrophotometric measurement of the dried particle samples was performed on Thermo, Nicolet 6700 FT-IR. XPS Spectra were recorded on Kratos AXIS Ultra DLD x-ray photoelectron spectrometer. All UV-Visible spectra were measured by Varian Cary 50 Probe UV-Visible spectrometer. All Fluorescence spectra were performed on Varian Eclipse Probe fluorescence spectrometer by personal computer data processing unit. The light source is Cary Eclipse pulsed xenon lamp and a detector is photomultiplier tube. The pH value was calibtrated with pH meter.

2.1.2 Materials

2-aminophenylboronic acid hydrochloride (2-APBA) and 4-aminophenylboronic acid hydrochloride (4-APBA) ≥95% were purchased from Aldrich. 3-aminophenylboronic acid hemisulfate (3-APBA) >98% and Glucose oxidase from Aspergillus niger were purchased from TCI. D (+)-Glucose anhydrous for biochemistry and Hydrogen peroxides (H_2O_2) 30% were obtained from Merck. HEPES (free acid) was obtained from OmniPur. All solutions were prepared and diluted by using ultrapure water with a resistivity of 18.2 MΩ from the Millipore Milli-Q system.

2.2 Synthesis and characterization

2.2.1 Synthesis experimental procedure

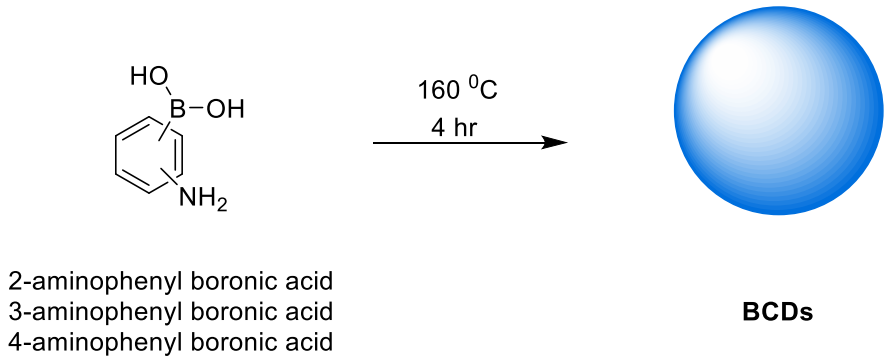

Figure 2.1 Preparation of the **BCDs** from three isomers of aminophenylboronic acid.

2.2.1.1 Synthesis of *o*-BCDs

Boronic acid functionalized carbon dots (**BCDs**) were prepared by one step hydrothermal carbonization. 2-aminophenylboronic acid hydrochloride (APBA) was used as a precursor for ***o*-BCDs**. 0.1 mmol of 2-APBA was dissolved in 5.00 mL H_2O. The solution was heated at 160°C for 4 h in the teflon-lined autoclave chamber. After cooling to room temperature, the solution was filtrated through a 0.22 µm microporous membrane and centrifuged at 10,000 rpm for 20 minutes to remove the large tracts. After filtration, the solution was dialyzed in a 2000 Da dialysis bag for 3 h to remove the inorganic salt. The resultant ***o*-BCDs** showed a colorless solution in daylight and a pale blue photoluminescence under UV irradiation.

2.2.1.2 Synthesis of *m*-BCDs

Boronic acid functionalized carbon dots (**BCDs**) were prepared by one step hydrothermal carbonization. 3-aminophenylboronic acid hemisulfate (APBA) was used as a precursor for ***m*-BCDs**. 0.1 mmol of 3-APBA was dissolved in 5.00 mL H_2O. The solution was heated at 160°C for 4 h. in the teflon-lined autoclave chamber. After cooling to room temperature, the solution was filtrated through a 0.22 µm microporous membrane and centrifuged at 10,000 rpm for 20 minutes to remove the large tracts. After filtration, the solution was dialyzed in a 2000 Da dialysis bag for 6 h to remove

the inorganic salt. The resultant ***m*-BCDs** showed a colorless solution in daylight and a blue photoluminescence under UV irradiation.

2.2.1.3 Synthesis of *p*-BCDs

Boronic acid functionalized carbon dots (**BCDs**) were prepared by one step hydrothermal carbonization. 4-aminophenylboronic acid hydrochloride (APBA) was used as a precursor for ***p*-BCDs**. 0.1 mmol of 4-APBA was dissolved in 5.00 mL H_2O. The solution was heated at 160°C for 4 h. in the teflon-lined autoclave chamber. After cooling to room temperature, the solution was filtrated through a 0.22 μm microporous membrane and centrifuged at 10,000 rpm for 20 minutes to remove the large tracts. After filtration, the solution was dialyzed in a 2000 Da dialysis bag for 3 h to remove the inorganic salt. The resultant ***p*-BCDs** showed a colorless solution in daylight and a pale blue photoluminescence under UV irradiation.

2.2.2 Characterization of BCDs

2.2.2.1 Size and morphology of BCDs

The morphology of **BCDs** was examined by transmission electron microscopy (TEM) and atomic force microscopy (AFM). TEM samples of each **BCDs** were prepared by ultra-sonication of **BCDs** solution to disperse the materials for 15 minutes. The droplet of the solution was placed onto carbon-coated copper grid. After 5 minutes, the droplet was removed by adsorbing to a piece of filter paper. The samples were dried and monitored by TEM. AFM samples of each **BCDs** were prepared by ultra-sonication of **BCDs** solution to disperse the materials for 15 minutes. A drop of the solution was placed on glass slide. The droplet of solution was spreaded by spin coating (spin speed 3000 ppm). After spin coating, AFM samples were dried overnight in -high vacuum chamber.

2.2.2.2 Compositions and functional groups of BCDs

To demonstrate the functional groups of **BCDs** with precursors. The as-prepared **BCDs** were characterized by FT-IR measurement with KBr plate method. The all samples of **BCDs** were dried in freeze dryer for 3 days prior to characterization. The composition of **BCDs** was investigated by X-ray photoelectron spectroscopy (XPS). The

dried samples were mounted on sample holder using TorrSeal epoxy and silver epoxy. Then, the samples were dried in ultrahigh vacuum chamber until the pressure reached to 10^{-7} torr and data were collected by XPS.

2.3 Optical property studies

2.3.1 UV-Vis spectroscopy system of BCDs (*o*-BCDs, *m*-BCDs, and *p*-BCDs)

50.00 µL of **BCDs** solution was mixed with 0.1 M HEPES buffer pH 7.4 to the final volume of 3.00 mL. Each solution was placed into a quartz cuvette with a path length of 1.0 cm. The UV spectra were recorded at room temperature.

2.3.2 The fluorescence system studies of BCDs (*o*-BCDs, *m*-BCDs, and *p*-BCDs)

In each experiment, solution of sensor molecules 50.00 µL were mixed with 0.1 M HEPES buffer pH 7.4 to the final volume 3.00 mL. The mixture solution was placed into a quartz cuvette with a path length of 1.0 cm. Fluorescence spectra were recorded at room temperature under the condition below.

Table 2.1 The optimal conditions for fluorescence measurement of **BCDs**.

	***o*-BCDs**	***m*-BCDs**	***p*-BCDs**
Excitation wavelength (nm)	280	310	270
Start (nm)	290	320	280
Stop (nm)	800	800	800
Width of excitation and emission slit (nm)	5	5	5
Smoothing factor	19	19	19
Scan rate	600 nm/min	600 nm/min	600 nm/min
PMT	670	570	700
Range of emission spectrum (nm)	310-410	330-480	300-450

2.3.3 Determination of quantum yield of BCDs (*o*-BCDs, *m*-BCDs, and *p*-BCDs)

The fluorescence quantum yield (Φ) is the ratio of photons absorbed to photons emitted through fluorescence between reference compound and unknown compound. In this work, quinine bisulfate was used as a reference compound in 0.5 M H_2SO_4.

2.00 µL of reference solution was mixed with 0.1M HEPES buffer pH7.4 to the final volume 2.00 mL. The mixture was recorded under UV-Vis spectroscopy and then was measured emission spectra at excitation wavelength of reference compound. The mixture was diluted to five concentrations which displayed the absorbance of < 0.01 au. and each portion was measured under UV-vis and fluorescence spectroscopy.

In the case of each **BCDs**, the measurement of fluorescence quantum yield was similarly determined by the reference solution as shown in table 2.2. The quantum yield of each **BCDs** was calculated by equation 3 as shown below.

Table 2.2 The absorbance and peak area of quinine bisulfate and **BCDs** for quantum yield measurement.

Types of **BCDs**	Times	Absorbance	Peak area
Quinine bisulfate	1	0.08363	67564.544
	2	0.06743	56237.121
	3	0.05185	44040.263
	4	0.03674	30792.353
	5	0.02758	24732.616
***o*-BCDs**	1	0.09157	3215.770
	2	0.08231	3128.705
	3	0.04628	1551.657
	4	0.03179	797.061
	5	0.02399	573.515
***m*-BCDs**	1	0.10004	22532.693
	2	0.06711	13901.883
	3	0.04350	8299.261
	4	0.03397	6480.907
	5	0.01771	3146.921
***p*-BCDs**	1	0.10045	3964.069
	2	0.079523	3028.434
	3	0.056828	2143.086
	4	0.038787	1046.654
	5	0.027511	732.8676

The quantum yield was determined by following equation

$$Q_x = Q_{std}\left(\frac{Grad_x}{Grad_{std}}\right)\left(\frac{n_x^2}{n_{std}^2}\right) \quad (3)$$

When Q_x = Quantum Yield of unknown

Q_{std} = Quantum Yield of reference compound

$Grad_x$ = slope of unknown

$Grad_{std}$ = slope of reference compound

n_x = refractive index of unknown solvent

n_{std} = refractive index of reference solvent

*peak area was determined by Micro Origin 6.0

2.3.4 The study of stability of BCDs (*o*-BCDs, *m*-BCDs, and *p*-BCDs)

Firstly, 50.00 μL of **BCDs** was added into quartz cuvette with a path length of 1.0 cm and then, the total volume was adjusted to 3.00 mL by using 0.1 M HEPES buffer solution. Fluorescence spectra were recorded for 1 month at room temperature under the optimal condition.

2.3.5 The studies on the effect of excitation wavelength

The stock solution of each **BCDs** was sonicated by ultra-sonication to disperse these particles for 15 minutes. After that, 50.00 μL of sensor molecules was mixed with 0.1 M HEPES buffer pH 7.4 to the final volume 3.00 mL. The solutions were placed into a quartz cuvette with a path length of 1.0 cm. Fluorescence spectra were recorded under various excitation wavelengths (250-350 nm) at room temperature.

2.3.6 The studies on the effect of pH

Table 2.3 The types of buffer solution at various pH and volume of the **BCDs** in total volume (3 mL).

pH	buffer	Volume of **BCDs** solution (μL)
3.6	0.1 M Acetate	50
4.0	0.1 M Acetate	50
5.0	0.1 M Acetate	50
6.0	0.1 M Phosphate	50
7.4	0.1 M HEPES	50
8.0	0.1 M HEPES	50
9.0	0.1 M Tris	50
10.0	0.1 M Tris	50

2.3.7 The reaction studies of the BCDs (*o*-BCDs, *m*-BCDs, and *p*-BCDs) with hydrogen peroxide using fluorescent titration experiment

2.3.7.1 The studies on the reaction time between BCDs and H_2O_2

The stock solution of each **BCDs** was sonicated by ultra-sonication to disperse these particles for 15 minutes. The 50.00 μL of sensor molecules were mixed with 0.1 M HEPES buffer pH 7.4. And then, the 0.1 M stock solution of H_2O_2 was added into the mixture solution as shown in table 2.4. The reaction time between **BCDs** and H_2O_2 was measured by fluorescence spectrometer with various times (0-60 minutes).

Table 2.4 The concentration of H_2O_2 for each **BCDs** (***o*-BCDs**, ***m*-BCDs**, and ***p*-BCDs**).

type of **BCDs**	Final concentration of H_2O_2 in 3 mL (mM)	Total volume (mL)	Volume of H_2O_2 (μL)
***o*-BCDs**	10.0	3.00	300
***m*-BCDs**	0.1	3.00	3
***p*-BCDs**	10.0	3.00	300

2.3.7.2 The fluorescent titration experiment

Typically, the stock solution of each **BCDs** was sonicated by ultra-sonication to disperse these particles for 15 minutes. And then, the 50.00 μL of sensor molecules was mixed with 0.1 M HEPES buffer pH 7.4. Next, the stock solution of H_2O_2 was added into the mixture solution as shown in table 2.5-2.7 for ***o*-BCDs**, ***m*-BCDs**, and ***p*-BCDs**, respectively. The fluorescence spectra were recorded after 15 minutes under excitation wavelength at 280, 310, and 270 nm for ***o*-BCDs**, ***m*-BCDs**, and ***p*-BCDs**, respectively.

Table 2.5 The concentration of H_2O_2 for ***o*-BCDs** system.

No.	Final concentration of H_2O_2 in 3 mL (mM)	Volume of H_2O_2 stock solution (μL)
1	2	1
2	10	5
3	20	10
4	40	20
5	59	30
6	79	40
7	98	50
8	156	80
9	193	100
10	304	160
11	375	200
12	545	300
13	706	400

Table 2.6 The concentration of H_2O_2 for ***m*-BCDs** system.

No.	Final concentration of H_2O_2 in 3 mL (mM)	Volume of H_2O_2 stock solution (μL)
1	0.1	3.0
2	0.2	6.0
3	0.5	15.0
4	0.7	21.0
5	1.0	30.0
6	2.0	60.0
7	5.0	150.0

Table 2.7 The concentration of H_2O_2 for ***p*-BCDs** system.

No.	Final concentration of H_2O_2 in 3 mL (mM)	Volume of H_2O_2 stock solution (μL)
1	0	0
2	10	30
3	25	75
4	50	150
5	75	225
6	100	300
7	150	400
8	200	600
9	250	750
10	300	900
11	400	1200
12	500	1500

2.3.8 The enzymatic studies of the BCDs

According to the reaction studies of the **BCDs** (***o*-BCDs**, ***m*-BCDs**, and ***p*-BCDs**) with hydrogen peroxide using fluorescent titration experiment, the results showed that ***m*-BCDs** have an excellent probe for H_2O_2 sensing. Thus, ***m*-BCDs** was chosen to be a represent of the other **BCDs** to optimal condition for enzymatic probe studies.

2.3.8.1 The studies on the effect of unit of glucose oxidase

Firstly, the 1 mM of glucose was added in each bottle that contained the different units of GOx in 0.1 M HEPES buffer pH 7.4 as shown in table 2.8-2.10. Next, the mixture solution was incubated at 37°C under O_2 condition for 60 minutes. And then, the 50.00 μL of **BCDs** was added and stirred 15 minutes. The fluorescence spectra were recorded under excitation wavelength at 280, 310 and 270 nm for ***o*-BCDs**, ***m*-BCDs** and ***p*-BCDs**, respectively.

Table 2.8 The final unit of glucose oxidase in total volume (3 mL) for ***o*-BCDs** system.

No.	Final unit of GOx in 3 mL (Unit)	Volume of 200 units/3mL GOx stock solution (μL)
1	1	15
2	3	45
3	10	150
4	20	300
5	50	750

Table 2.9 The final unit of glucose oxidase in total volume (3 mL) for ***m*-BCDs** system.

No.	Final unit of GOx in 3 mL ($mmol/dm^3$)	Volume of 422 units/mL GOx stock solution (μL)
1	1	2.5
2	3	7.0
3	6	14.0
4	15	37.5

Table 2.10 The final unit of glucose oxidase in total volume (3 mL) for ***p*-BCDs** system.

No.	Final unit of GOx in 3 mL ($mmol/dm^3$)	Volume of 200 units/mL GOx stock solution (μL)
1	1	5
2	3	15
3	30	150
4	60	300
5	120	600
6	240	1200
7	360	1800

2.3.8.2 The studies on the effect of enzymatic reaction time

In this work, ***m*-BCDs** was chosen to be the fluorescence probe for choice via enzymatic reaction due to highly effective sensing aspect. The 200.00 μL of 1 mM glucose and 1 unit of GOx were mixed and incubated at 37°C under O_2 for 60 minutes. And then, the 50.00 μL of **BCDs** was added into the mixture solution and stirred for 15 minutes. The enzymatic reaction time was measured by fluorescence spectroscopy under excitation wavelength of 310 nm with various times (0-120 minutes).

2.3.8.3 The titration studies of glucose in enzymatic reaction

Typically, the 1 unit of GOx was added in each portion that contained the different concentration of glucose in 0.1 M HEPES buffer pH 7.4 as shown in table 2.11-2.13. Next, the mixture solution was incubated at 37°C under O_2 for 60 minutes. The stock solution of each **BCDs** was sonicated by ultra-sonication to disperse these particles for 15 minutes. And then, the 50.00 μL of sensor molecules was pipetted into the mixture solution and stirred for 15 minutes. The fluorescence spectra were recorded under excitation wavelength of 280, 310, and 270 nm for ***o*-BCDs**, ***m*-BCDs** and ***p*-BCDs**, respectively.

Table 2.11 The final concentration of glucose in total volume (3 mL) for ***o*-BCDs** system.

No.	Final concentration of glucose in 3 mL (mM)	Volume of 1.43 M glucose stock solution (μL)	Volume of 128 units/mL GOx stock solution (μL)
1	20	42.0	7.8
2	40	84.0	7.8
3	60	126.0	7.8
4	80	167.8	7.8
5	100	209.8	7.8
6	156	314.7	7.8
7	200	419.6	7.8
8	300	629.4	7.8
9	400	839.2	7.8
10	545	1143.0	7.8

Table 2.12 The final concentration of glucose in total volume (3 mL) for ***m*-BCDs** system.

No.	Final concentration of glucose (mM)	Volume of 191 mM glucose stock solution (μL)	Volume of 120 units/mL GOx stock solution (μL)
1	0.2	3.1	8.3
2	0.4	6.3	8.3
3	0.6	9.4	8.3
4	0.8	12.6	8.3
5	1	15.7	8.3
6	2	31.4	8.3
7	3	47.1	8.3
8	4	62.8	8.3
9	5	78.5	8.3
10	10	125.7	8.3
11	15	157.0	8.3
12	20	235.6	8.3

Table 2.13 The final concentration of glucose in total volume (3 mL) for ***p*-BCDs** system.

No.	Final concentration of glucose (mM)	Volume of 1 M glucose stock solution (μL)	Volume of 100 units/mL GOx stock solution (μL)
1	20	60.0	30.0
2	100	300.0	30.0
3	300	900.0	30.0
4	450	1350.0	30.0
5	600	1800.0	30.0
6	750	2250.0	30.0

CHAPTER III

RESULTS AND DISCUSSION

3.1 Design concept of enzymatically activated sensor for glucose oxidase

Diabetes mellitus is one of the biggest public health threats. There have been minority effectively direct methods for selective glucose detection via non-enzymatic methods. Thus, the determination of H_2O_2 is an alternative method that can be generated from glucose oxidase (GOx) enzymatic reactions [14, 36-38]. The H_2O_2 plays a significant and important role for screening and diagnosis. The concentration of H_2O_2 may be used as an indicator of the progress of enzymatic approach. Recently, several techniques are available for H_2O_2 detection including fluorometric [39-41], colorimetric [42-44] and electrochemical analysis [45-49]. In addition, carbon dots (CDs) is a new green popular material owing to their advantages, such as low cytotoxicity and a good biocompatibility. It has been used in various applications. Among the development of glucose sensing molecules, fluorescence probe based on boronic acid was widely focused as a recognition molecule to determine monosaccharide due to the fact that boronic acid specifically bound with *cis*-diol of saccharide such as glucose and fructose resulting in fluorescence changing. The determination of concentration of glucose through fluorescence changing is the one of famous method. Consequently, this research aims to design, develop and synthesize a new boronic acid functionalized carbon dots for determination of glucose through enzymatic reaction. The conceptual design of this study was illustrated in scheme 3.1.

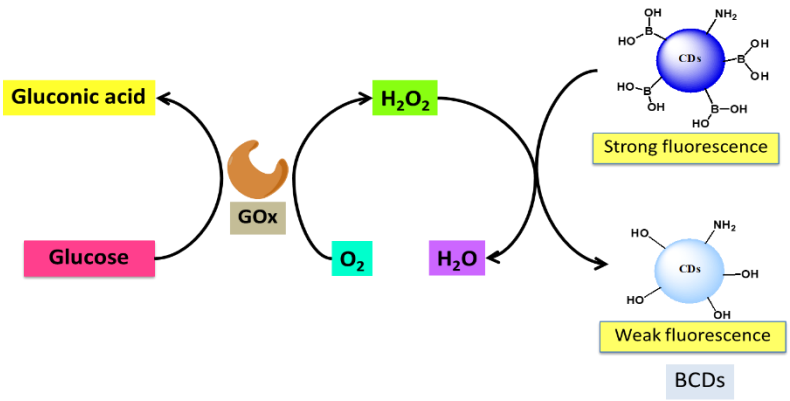

Scheme 3.1 The conceptual illustration of **BCDs** for detection of glucose through enzymatic mechanism.

3.2 Characterizations of all BCDs

3.2.1 Fourier Transform Infrared Spectroscopy (FT-IR) analysis of BCDs

To characterize the functional group on **BCDs** structure, Fourier Transform Infrared Spectroscopy (FT-IR) was investigated as shown in figure 3.1.

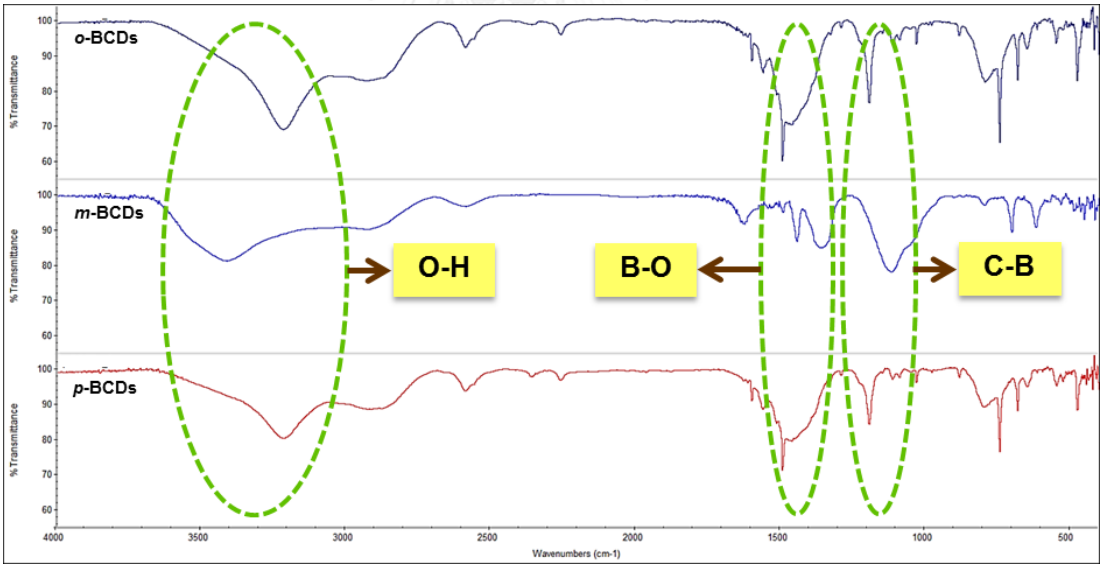

Figure 3.1 FT-IR spectra of all **BCDs**.

According to FT-IR measurement, FT-IR spectra of three isomers **BCDs** did not show a clear illustration of molecule. The FT-IR spectra of ***o*-BCDs** and ***p*-BCDs** showed the peaks at about 3200, 1500, and 1170 cm^{-1} corresponding to the characteristics O-H stretching mode, B-O stretching mode, and C-B stretching mode, respectively.

Similarly, the ***m*-BCDs** showed the peak at 3431, 1410, and 1100 cm^{-1} which were characteristics of functional group of ***o*-BCDs** and ***p*-BCDs**. Deeply considering, the whole FT-IR spectrum of ***m*-BCDs** exhibited the different feature compared to those of ***o*-BCDs** and ***p*-BCDs**. This proposed the different structure of ***m*-BCDs** from ***o*-BCDs** and ***p*-BCDs** which should be elucidated by other technique. However, these results can be confirmed that **BCDs** was successfully synthesized from APBA.

3.2.2 Transmission electron microscopy (TEM) analysis of BCDs

To examine the morphology of **BCDs**, TEM images of **BCDs** were investigated as shown in table 3.1.

Table 3.1 TEM images and particle size distribution of ***o*-BCDs**, ***m*-BCDs** and ***p*-BCDs**.

o-BCDs	*m*-BCDs	*p*-BCDs
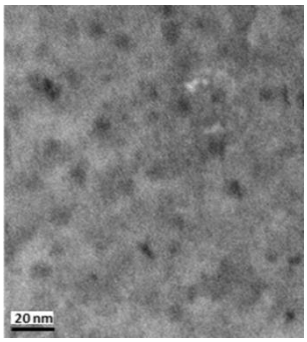	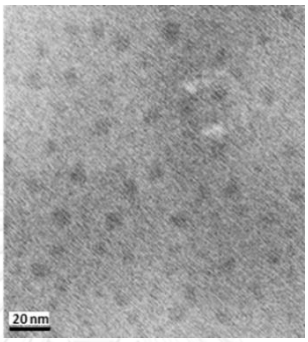	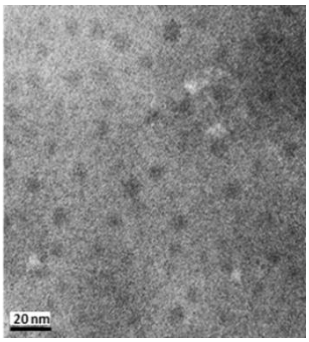
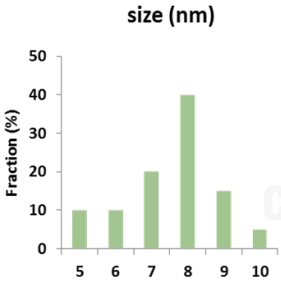	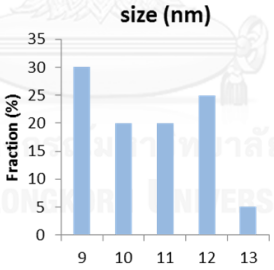	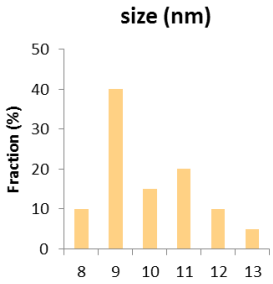

According to TEM analysis, three materials (***o*-BCDs**, ***m*-BCDs** and ***p*-BCDs**) displayed spherical morphology nanoparticles. The ***o*-BCDs** and ***p*-BCDs** showed fairly uniform nanoparticles with the average diameter sizes of approximately 8 nm and 9 nm, respectively. In the case of ***m*-BCDs**, the particle sizes varied from 9-12 nm (calculated 20 particles from TEM image by using ImageJ software).

3.2.3 Atomic force microscopy (AFM) analysis of BCDs

To the best of our understanding, graphene quantum dots (GQDs) are the graphene sheets smaller than 10 nm. They possess one or a few layers of graphene sheet which connects chemical groups on the edges. The single layer sheet of graphene shows the thickness less than 1 nm [50]. Actually, to verify the number of graphene layer, AFM was used to investigate the topographic properties of **BCDs** as shown in table 3.2.

Table 3.2 AFM images of ***o*-BCDs**, ***m*-BCDs** and ***p*-BCDs**.

Types of **BCDs**	AFM image	Thickness (nm)
***o*-BCDs**	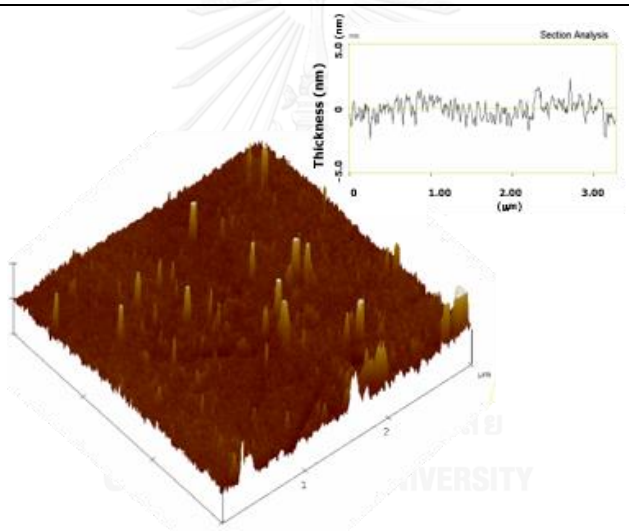	0.6-0.8
***m*-BCDs**	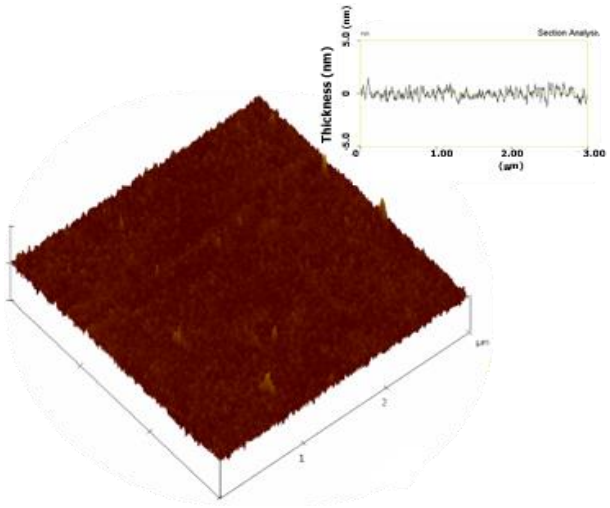	0.5-1.0

***p*-BCDs**	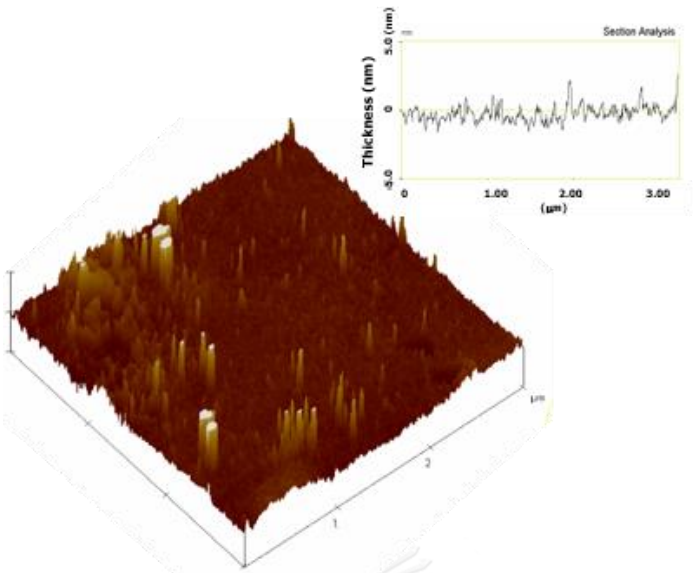	0.5-0.9

From the AFM analysis (Table 3.2), AFM images exhibited a typical topographic height of all three materials including ***o*-BCDs**, ***m*-BCDs** and ***p*-BCDs**. The thickness of graphene sheet of these materials was approximately 0.5-1.0 nm. These results clearly indicated that the **BCDs** showed the single layer of graphene feature.

3.2.4 Nuclear magnetic resonance of boron (^{11}B-NMR) of BCDs

The new material of **BCDs** was synthesized via carbonization process by using boronic acid derivative as a starting material. The ^{11}B-NMR spectroscopy was examined to confirm the boron site of nanomaterials. To elucidate the boron position in ***o*-BCDs** structure, the 2-aminophenylboronic acid (***o*-**APBA) as the starting compound was also measured for comparison. Based on ^{11}B-NMR spectrum of ***o*-**APBA in figure 3.2a, the boron peak at 27.3 ppm corresponding to B-OH of boronic acid was observed. The case of ***o*-BCDs** showed the main peak at 18.5 ppm and minor peak at 19.1 ppm (Figure 3.2b). In our hypothesis, this peak at 18.5 may be the B-O of boric acid (B_2O_3). To clarify the boron site of ***o*-BCDs**, the ^{11}B-NMR spectrum of boric acid (B_2O_3) was also recoded and showed the main peak at 18.5 ppm and minor peak at 19.1 ppm (Figure 3.2c). The results revealed that the synthesized ***o*-BCDs** consisted of the B-O group in its structure.

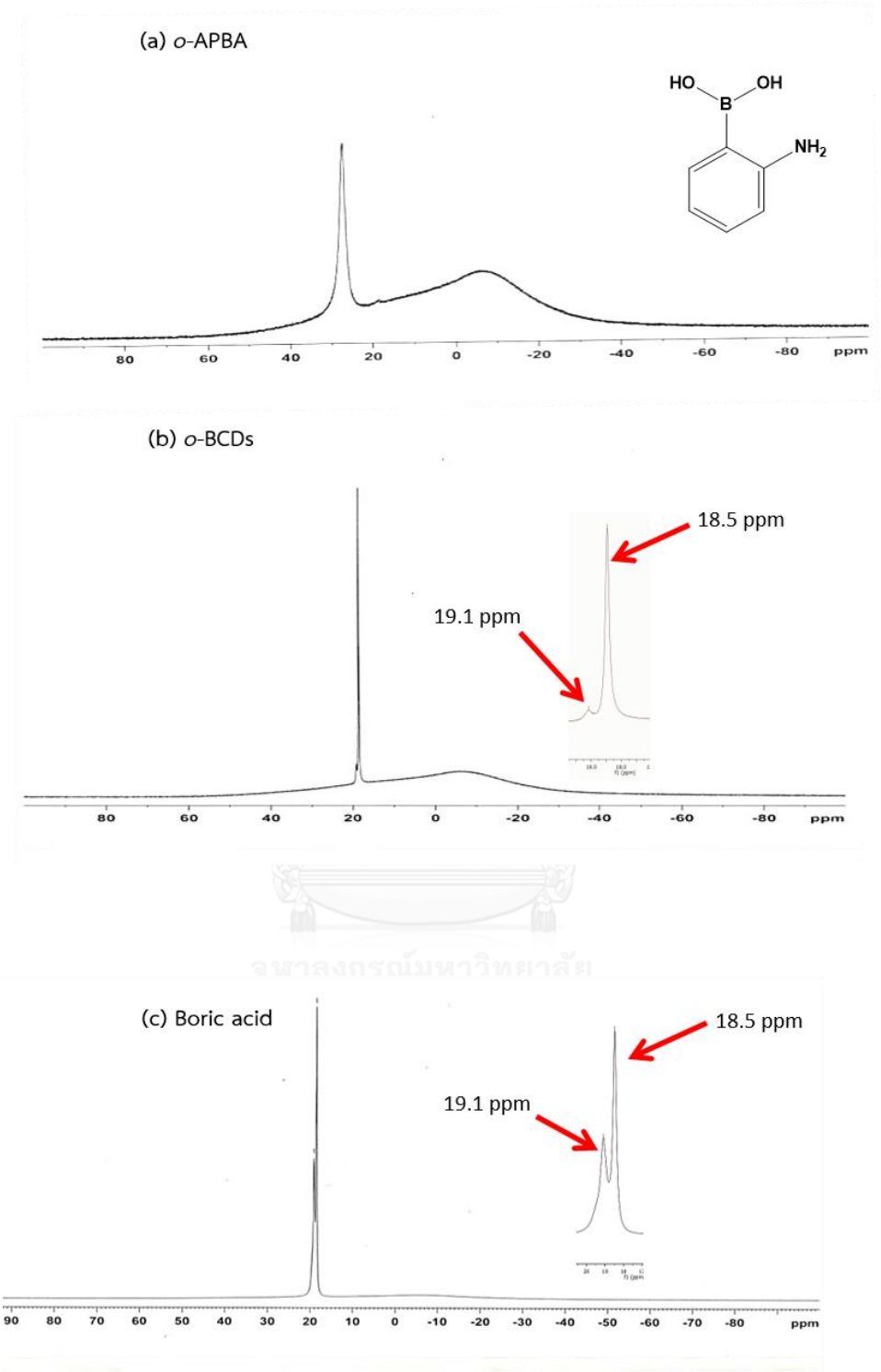

Figure 3.2 The ^{11}B-NMR spectra of ***o*-**APBA (a), ***o*-BCDs** (b) and boric acid (c).

The structure of ***m*-BCDs** was examined by ^{11}B-NMR spectroscopy which was compared to the ^{11}B-NMR spectrum of 3-aminophenylboronic acid (***m*-**APBA) as a

starting compound. The boron peak of ***m*-BCDs** was appeared at 28.8 ppm which is consistent with the boron peak at 28.6 ppm of ***m*-**APBA assigned to boronic acid group (B-OH) as shown in the figure 3.3. It clearly confirmed that the ***m*-BCDs** contained boronic acid group at the edge of graphene sheet.

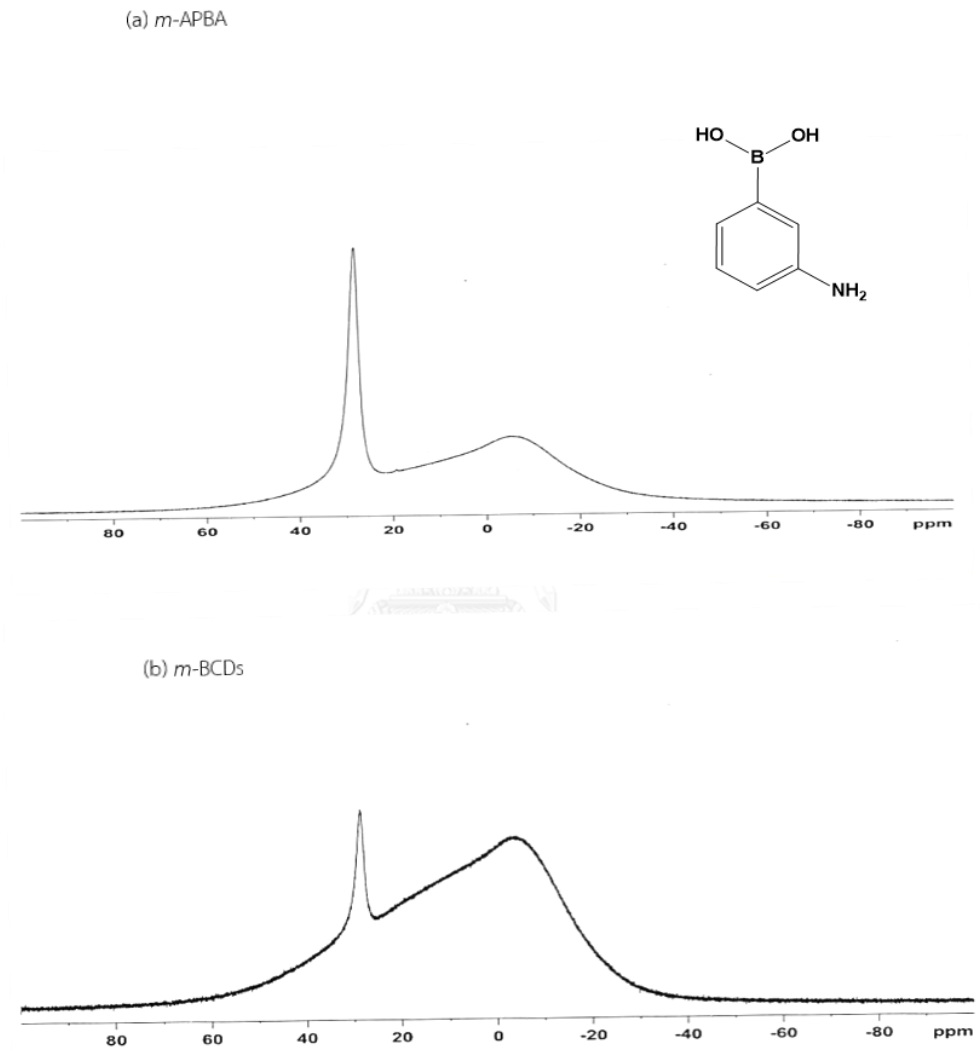

Figure 3.3 The ^{11}B-NMR spectra of ***m*-**APBA (a) and ***m*-BCDs** (b).

In the case of ***p*-BCDs**, the 4-aminophenylboronic acid (***p*-**APBA) was used a reference compound that was partially decomposed to boric acid. As the results, the ^{11}B-NMR spectra of ***p*-**APBA represented the main peak at 28.9 ppm and minor peak at

19.4 ppm, corresponding to B-OH of boronic acid and B-O of boric acid (B_2O_3), respectively. Unfortunately, the ***p*-BCDs** showed the boron peak at 19.4 ppm corresponding to B-O of boric acid. This result confirmed that ***p*-BCDs** did not consist of boronic acid group at the edge of graphene sheet. However, it consisted of boron doped in the structure.

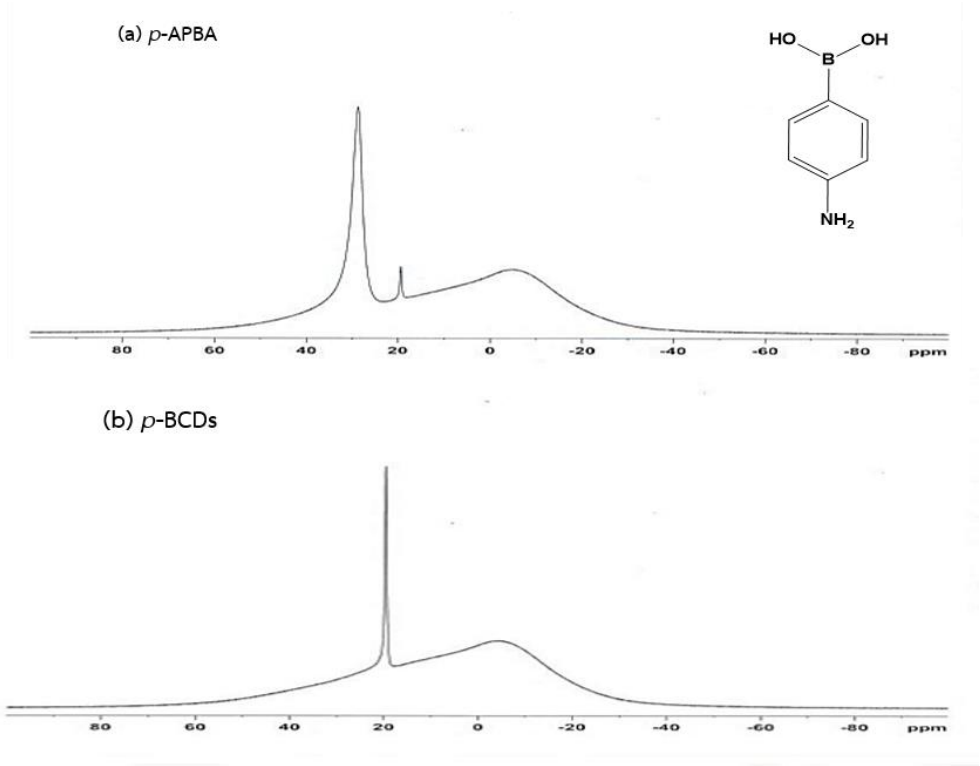

Figure 3.4 The ^{11}B-NMR spectra of ***p*-**APBA (a) and ***p*-BCDs** (b).

3.2.5 X-ray photoelectron spectroscopy (XPS)

Furthermore, to gain more information about structure of the prepared **BCDs**, the chemical compositions of the three materials (***o*-BCDs**, ***m*-BCDs** and ***p*-BCDs**) were also investigates by x-ray photoelectron spectroscopy as shown in figure 3.5-3.7.

The new material of **BCDs** was synthesized via carbonization process by using boronic acid derivative as a starting material. The XPS full scan spectrum of ***o*-BCDs** presented four main peaks of B_{1s}, C_{1s}, N_{1s} and O_{1s} at 192.8 eV, 284.8 eV, 400.8 eV and 532.8 eV, respectively. It can be suggested that ***o*-BCDs** consisted of B, C, N and O elements in the structure. Deeply considering, the C 1s scan spectrum exhibited the characteristic of four peaks including C-B at 284.184 eV, sp^2-C and C-C at 284.911 eV, C-O at 285.757 eV indicating the abundant carbon structure and the peak at 286.739 eV of C-N confirms the existence of numerous nitrogen containing group as shown in figure 3.5b. Interestingly, B 1s spectrum showed only one characteristic peak at 193.778 eV assigned to the B-O of B_2O_3 (Figure 3.5c). With consistent of ^{11}B-NMR data, this result clearly confirmed the disappearance of boronic acid on the edge of graphene sheet of ***o*-BCDs**. Moreover, the N 1s scan spectrum demonstrated the types of nitrogen pyridinic (399.216 eV), primary amine (400.781 eV), quaternary amine (402.174 eV) and pyridine oxide (403.344 eV) as shown in figure 3.5d. This information suggested that ***o*-BCDs** comprised the primary amine and quaternary amine as well as B-O of B_2O_3 group in the structure.

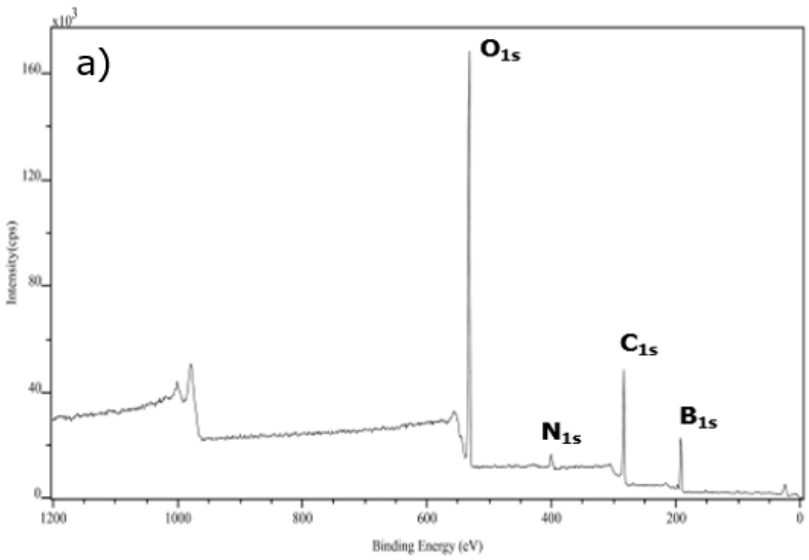

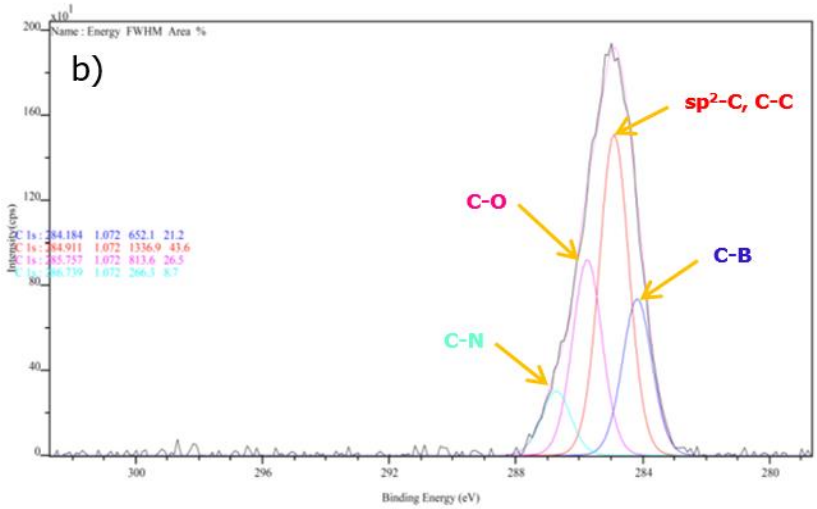

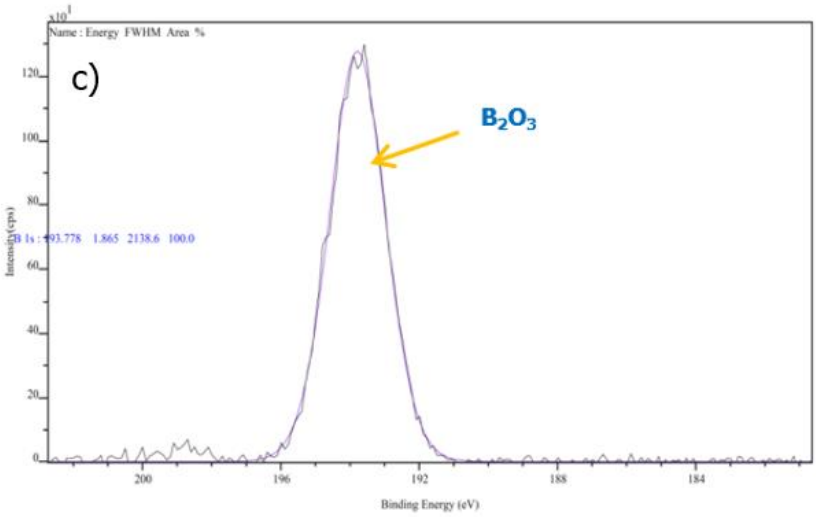

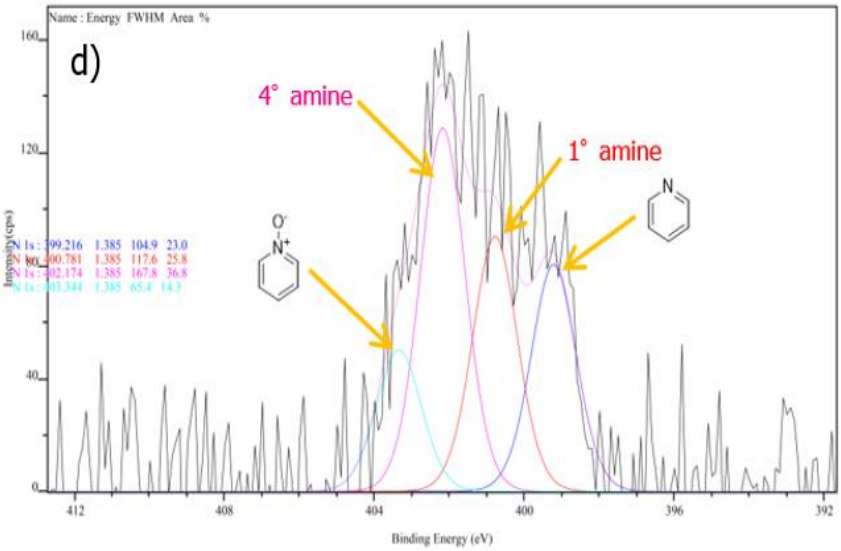

Figure 3.5 XPS spectra of the ***o*-BCDs** (a), high resolution C1s (b), B1s (c), N1s (d) peaks of the ***o*-BCDs**.

The chemical compositions of ***m*-BCDs** were investigated as shown in figure 3.6. The XPS scan spectrum of ***m*-BCDs** demonstrated the binding energies of each element in the material. The C 1s scan spectrum displayed the characteristics of four peaks inducing C-B at 283.50 eV, C-C at 284.31 eV, sp^2-C at 284.96 eV indicating the abundant carbon structure. The peak at 285.86 eV of C-N confirms the existence of numerous nitrogen containing group as shown in figure 3.6a. The B 1s spectrum showed two peaks including BC_2O at 191.41 eV and B-OH at 191.99 eV, assigned to the B-O of boronic acid group (Figure 3.6b). As the ^{11}B-NMR data mentioned previously, it clearly confirmed the existence of boronic acid on the edge of graphene sheet of ***m*-BCDs**. In the addition, the N 1s scan spectrum consisted of types of nitrogen primary amine at 400.05 eV and quaternary amine at 401.61 eV (Figure 3.6c). These data insisted the good evidence for ***m*-BCDs** containing B-O bonding of boronic acid and nitrogen atom in form of primary amine and quaternary amine in its structure.

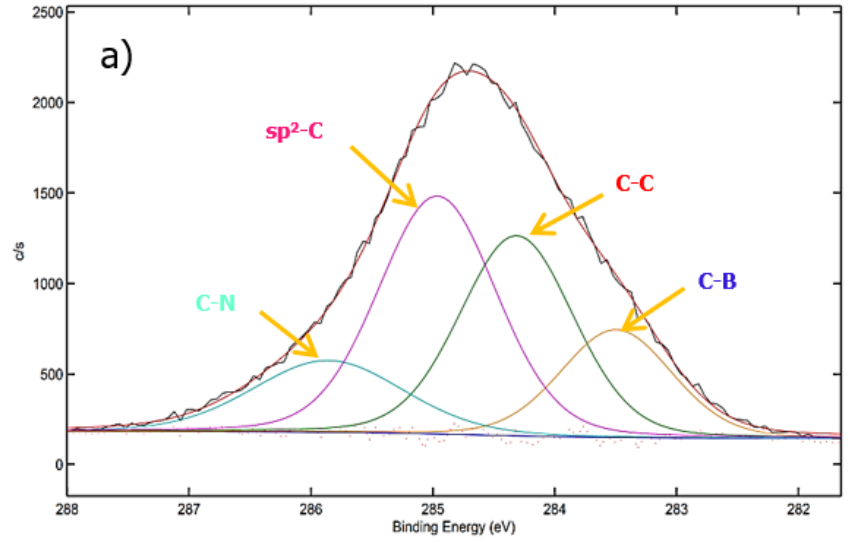
a)
sp²-C
C-C
C-B
C-N
c/s
Binding Energy (eV)

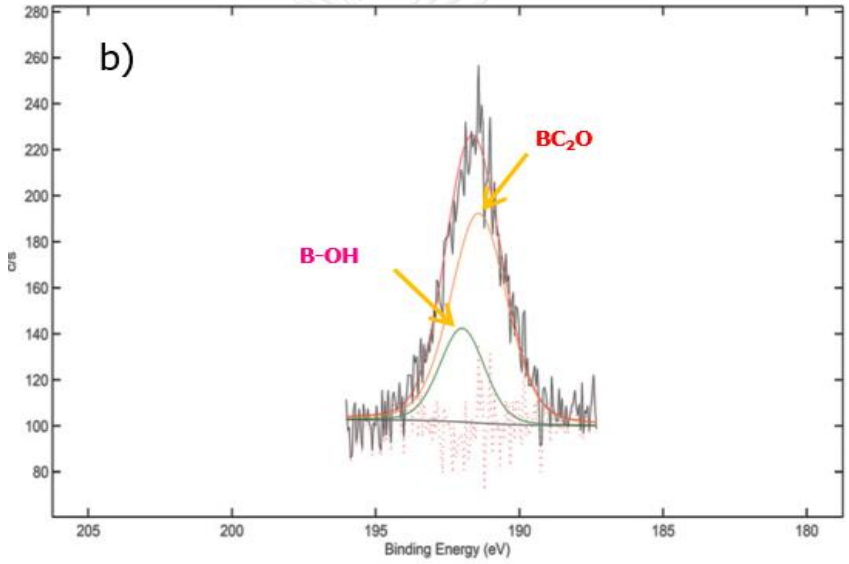
b)
BC₂O
B-OH
c/s
Binding Energy (eV)

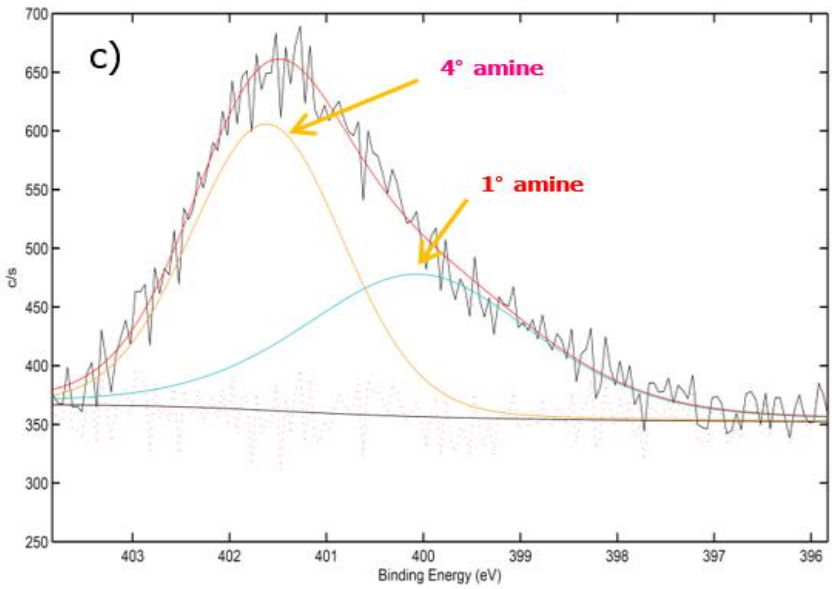

Figure 3.6 XPS spectra of the ***m*-BCDs** (a), high resolution C1s (b), B1s (c), N1s (d) peaks of the ***m*-BCDs**.

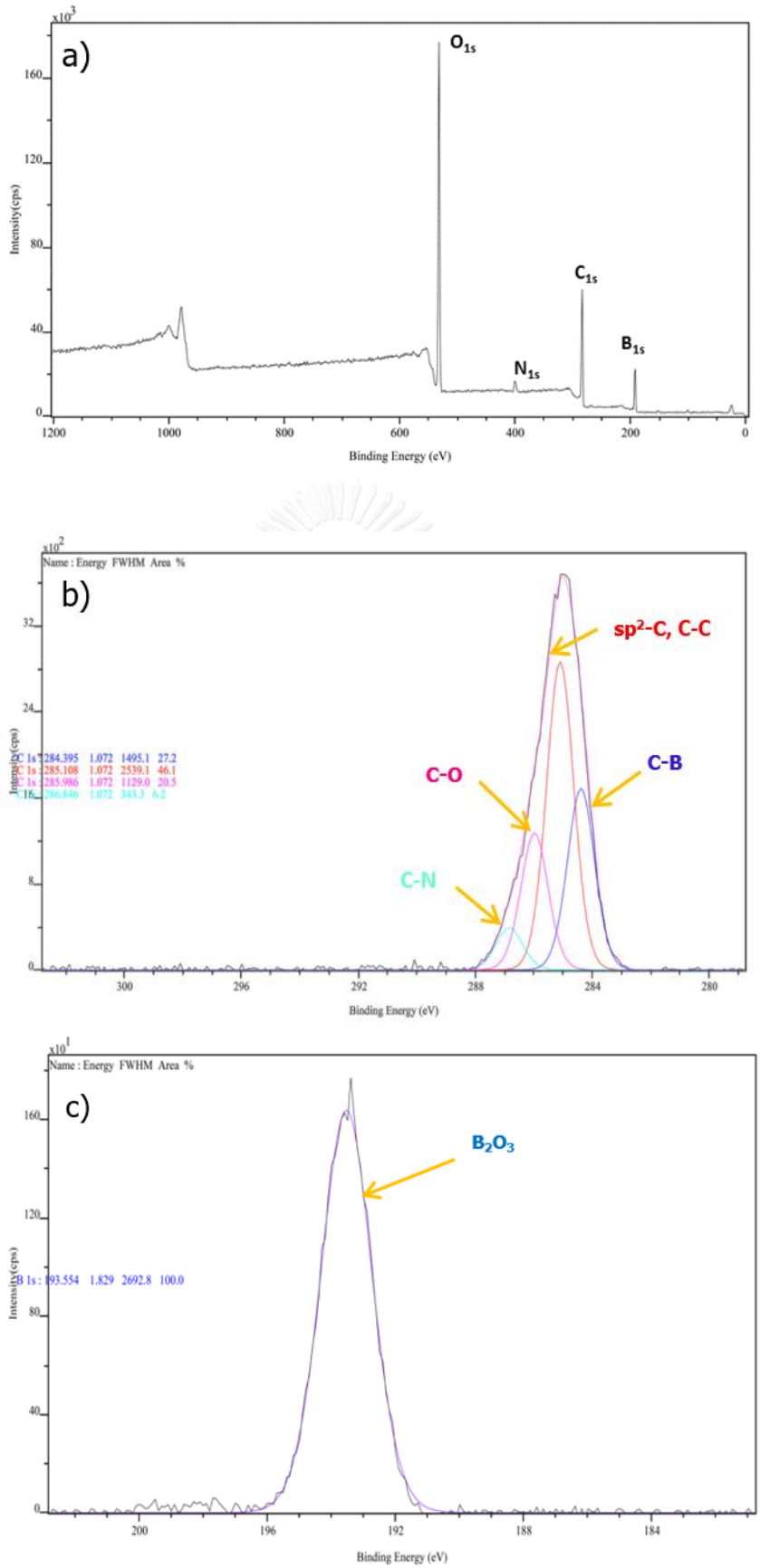
a)
O1s
C1s
B1s
N1s
Intensity(cps)
Binding Energy (eV)
b)
Name : Energy FWHM Area %
sp2-C, C-C
C-O
C-B
C-N
C 1s : 284.395 1.072 1495.1 27.2
C 1s : 285.108 1.072 2539.1 46.1
C 1s : 285.986 1.072 1129.0 20.5
C 1s : 286.846 1.072 343.3 6.2
Intensity(cps)
Binding Energy (eV)
c)
Name : Energy FWHM Area %
B2O3
B 1s : 193.554 1.829 2692.8 100.0
Intensity(cps)
Binding Energy (eV)

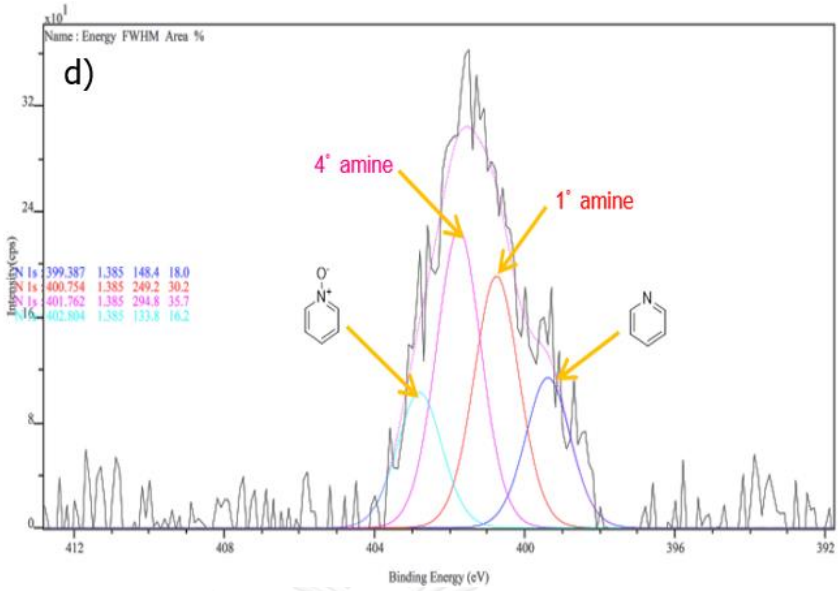

Figure 3.7 XPS spectra of the ***p*-BCDs** (a), high resolution C1s (b), B1s (c), N1s (d) peaks of the ***p*-BCDs**.

The chemical compositions of the ***p*-BCDs** were illustrated in figure 3.7. The XPS full scan spectrum of ***p*-BCDs** demonstrated the binding energy of each element in materials including four main peaks of B_{1s}, C_{1s}, N_{1s} and O_{1s} at 192.8 eV, 284.8 eV, 400.8 eV and 532.8 eV, respectively. These results revealed the elements of B, C, N and O exiting in ***p*-BCDs** structure. Deeply considering, the C 1s scan spectrum showed the characteristics of four peaks including C-B at 284.395 eV, sp^2-C and C-C at 285.108 eV, C-O at 285.986 eV and C-N at 286.846 eV as shown in figure 3.7b. The B 1s scan spectrum exhibited only one peak at 193.554 eV assigned to the B-O of B_2O_3 (Figure 3.7c). With consistent of ^{11}B-NMR data, this result clearly confirmed the disappearance of boronic acid on the edge of graphene sheet of ***p*-BCDs**. Furthermore, the N 1s scan spectrum demonstrated the nitrogen atom of pyridinic (399.387 eV), primary amine (400.754 eV), quaternary amine (401.762) and pyridine oxide (402.804 eV) as shown in figure 4.7d. This information indicated that ***p*-BCDs** structure comprised the primary amine and quaternary amine.

It is implied that no B-OH bonding of boronic acid existed on the edge of material in case of ***o*-BCDs** and ***p*-BCDs**. Based on the results mentioned above, the

novel materials synthesized from boronic acid derivative consisted of several types of functionalized graphene quantum dots (GQDs) such as boronic acid, primary amine, and quaternary amine existing on the graphene sheet. From the XPS and ^{11}B-NMR analysis, the structure of ***o*-BCDs** and ***p*-BCDs** demonstrated the B-O of boric acid. It means that no B-OH moiety on the edges of graphene sheet for ***o*-** and ***p*-BCDs**. Interestingly, the ***m*-BCDs** showed the existence of B-OH group on the edges of graphene sheet. This suggested that all **BCDs** consist of boron and nitrogen atom doped in their structures. However, we still expected that the different bonding of boron center enables to react with H_2O_2 generated from GOx enzymatic reaction to further determine the glucose concentration.

3.3 Optical property studies of N/B doped CDs

Three isomers of **BCDs** were investigated in the optical properties by using the UV-visible and fluorescence spectroscopy. The absorption bands of ***o*-BCDs** at 230 nm and 281 nm was observed. In the case of ***m*-BCDs**, the absorption peak presented about 205 nm, 244 nm and 303 nm. While ***p*-BCDs** was appeared at 230 nm and 290 nm as shown in the figure 3.8. This suggested the different structure of ***o*-**, ***m*-** and ***p*-BCDs** obtained from different isomer of APBA.

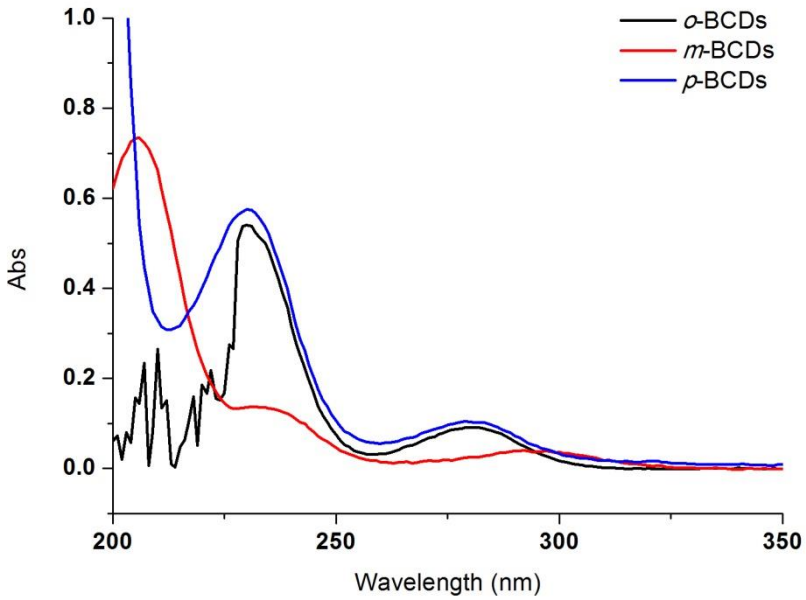

Figure 3.8 The absorption spectra of ***o*-BCDs** (black line), ***m*-BCDs** (red line) and ***p*-BCDs** (blue line).

The fluorescence spectra of ***o*-**, ***m*-** and ***p*-BCDs** were recorded under different excitation wavelength at 280 nm, 310 nm and 270 nm, respectively. As seen in the figure 4.9, the emission spectra of ***o*-**, ***m*-** and ***p*-BCDs** exhibited at 345 nm, 375 nm and 343 nm, respectively. Surprisingly, the emission bands of ***o*-** and ***p*-BCDs** addressed at the same wavelength and intensity. Particular of ***m*-BCDs** exhibited higher intensity and longer emission band than ***o*-** and ***p*-BCDs** did. Moreover, under UV light at 365 nm, these materials showed a blue brightness, especially ***m*-BCDs** showing the strongest blue brightness emission.

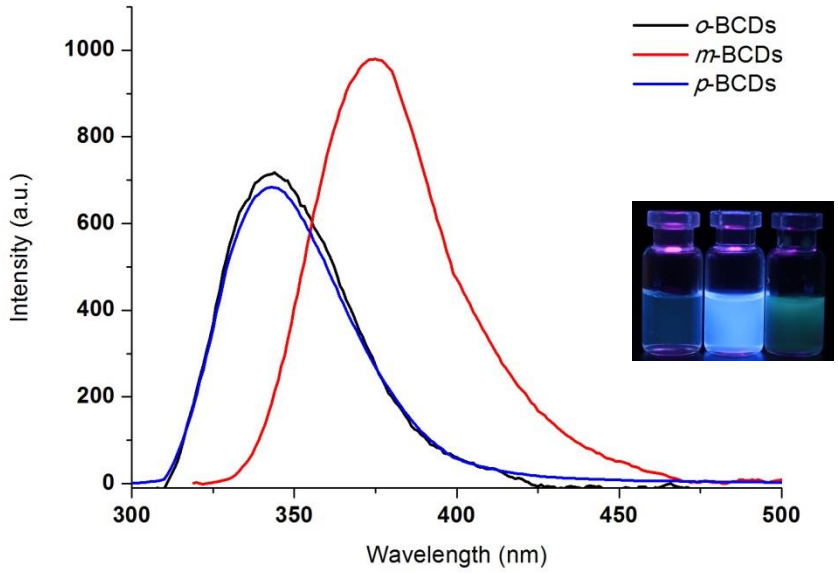

Figure 3.9 Fluorescence spectra of ***o*-BCDs** (black line), ***m*-BCDs** (red line) and ***p*-BCDs** (blue line). Inset: The ***o*-**, ***m*-** and ***p*-BCDs** under UV light at 365 nm (from left to right).

3.3.1 Quantum Yield (Φ) of all BCDs

Apart of fluorescence properties of all **BCDs**, we further measured the quantum yield (Φ) of all **BCDs** by using quinine bisulfate as a reference compound. The quantum yields of ***o*-BCDs**, ***m*-BCDs** and ***p*-BCDs** were shown in table 3.3.

Table 3.3 The quantum yield of ***o*-BCDs**, ***m*-BCDs** and ***p*-BCDs**.

***o*-BCDs**	$Q_x=0.58\left(\frac{41,394.51}{778,313.26}\right)\left(\frac{1.3325^2}{1.3367^2}\right)$	Q_x =**3.02%**
***m*-BCDs**	$Q_x=0.58\left(\frac{236,597.96}{778,313.26}\right)\left(\frac{1.3325^2}{1.3367^2}\right)$	Q_x=**17.26%**
***p*-BCDs**	$Q_x=0.58\left(\frac{45,282.94}{778,313.26}\right)\left(\frac{1.3325^2}{1.3367^2}\right)$	Q_x=**3.30%**

The quantum yield is a quantitative fluorescence of sensory molecules. These sensory molecules (***o*-BCDs**, ***m*-BCDs** and ***p*-BCDs**) were monitored by UV-vis spectroscopy and fluorescence spectroscopy by using quinine bisulfate as a reference compound for quantum yield studies. The results showed that the high quantum yield of meta-nitrogen/boron doped CDs (***m*-BCDs**) was up to 17.26% which was much higher than ortho- and para- nitrogen/boron doped CDs (only 3.02% and 3.30%, respectively). Interestingly, the quantum yield of ***m*-BCDs** was higher than typical carbon dot. As anticipated, the different substitution of B and N atom based starting materials would produce the different N/B doped structure of carbon dots inducing the photophysical-dependent properties of CDs.

3.3.2 The study of stability of BCDs (*o*-BCDs, *m*-BCDs and *p*-BCDs)

To verify the stability of **BCDs**, the fluorescence intensity of ***o*-**, ***m*-** and ***p*-BCDs** were recorded at various time by fluorescence spectroscopy at different PMT (670 for ***o*-BCDs**, 570 for ***m*-BCDs** and 700 for ***p*-BCDs**) for 1 month. The results showed that fluorescence intensity of each **BCDs** (***o*-BCDs** at 345 nm, ***m*-BCDs** at 375 nm and ***p*-BCDs** at 343 nm) was also remained constant (Figure 3.10). It means that fluorescence properties of all **BCDs** are stable in aqueous solution. Owing to these outstanding properties, the prepared **BCDs** serve as an attractive nanomaterial for sensing application.

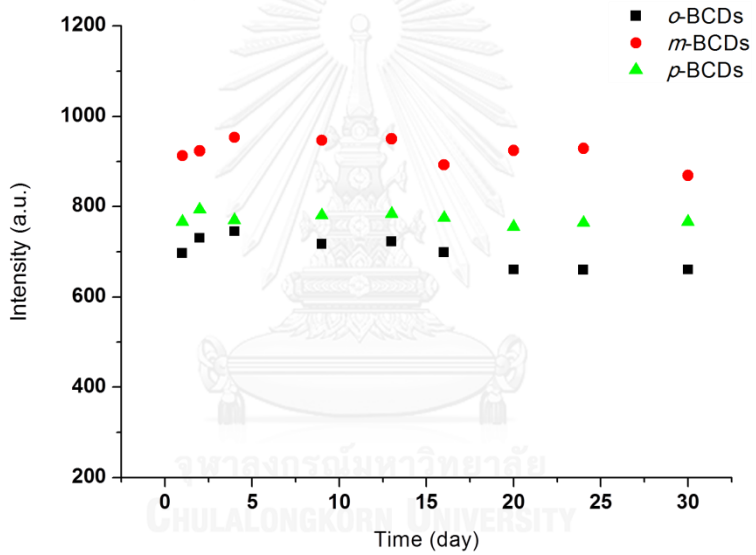

Figure 3.10 Fluorescence stability of ***o*-BCDs**, ***m*-BCDs** and ***p*-BCDs**.

3.3.3 The excitation wavelength studies of BCDs

To verify the excitation wavelength of **BCDs**, the fluorescence spectra were recorded at different excitation wavelength from 250 to 350 nm. The fluorescence feature of ***o*-BCDs** still demonstrated at 345 nm as a function of various excitation wavelength. Likewise, the emission bands of ***m*-BCDs** and ***p*-BCDs** exhibited at 375 nm and 343 nm, respectively, at various excitation wavelength in figure 3.11. The results revealed that these materials displayed the excitation-independent properties. Particular of the highest fluorescent intensities of ***o*-BCDs**, ***m*-BCDs** and ***p*-BCDs** were

addressed at excitation wavelength of 280, 310 and 270 nm, respectively. Thus, these excitation wavelengths were chosen for further sensing experiment of each **BCDs**.

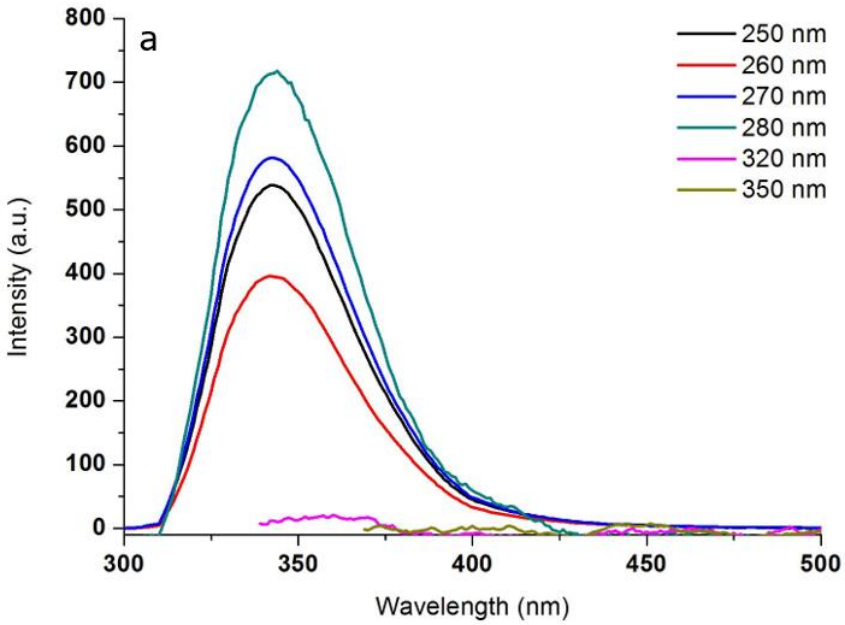

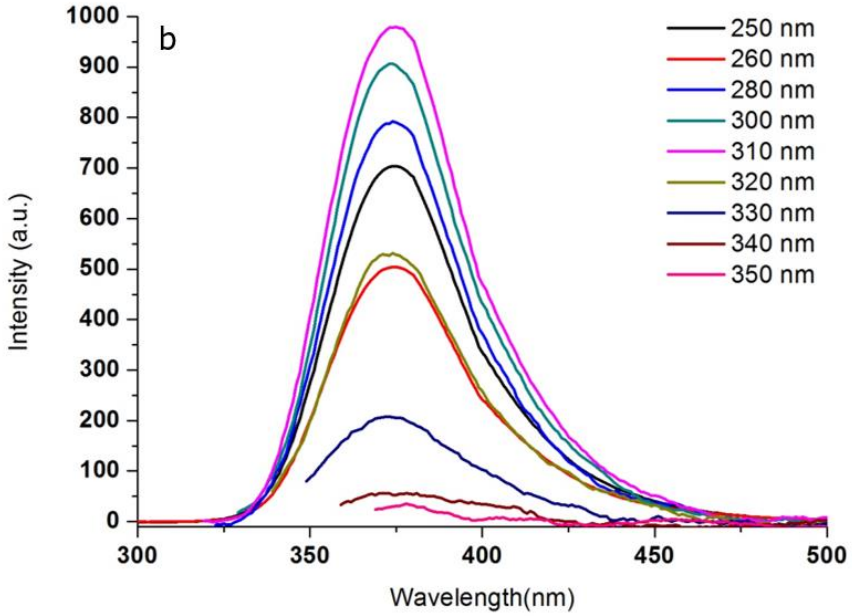

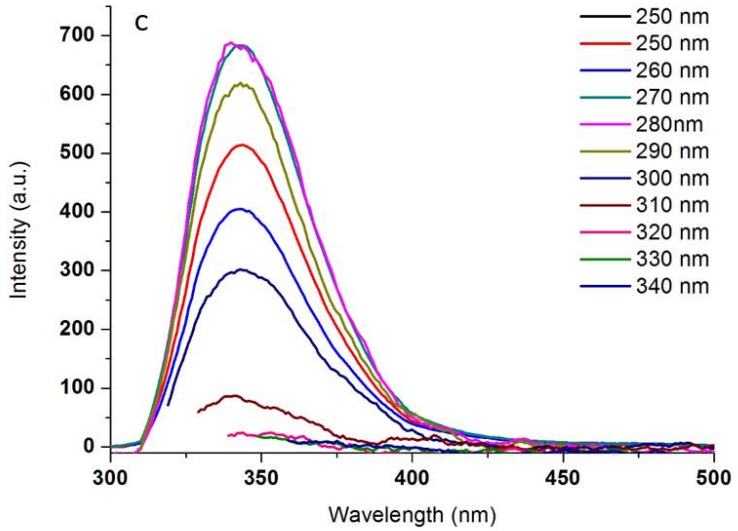

Figure 3.11 Fluorescence spectra of ***o*-BCDs** (a), ***m*-BCDs** (b) and ***p*-BCDs** (c) at different excitation wavelength (250-350 nm).

3.3.4 The studies on the effect of pH

The pH is a crucial role for fluorescence study of sensors. To optimize pH effect of fluorescence system, the fluorescence intensities of all **BCDs** (***o*-BCDs**, ***m*-BCDs** and ***p*-BCDs**) were examined in the pH range of 3.6-10. The emission bands of these materials were monitored at 345, 375 and 343 nm for ***o*-BCDs**, ***m*-BCDs** and ***p*-BCDs**, respectively. From the results, the highest fluorescence intensity displayed at the pH of 6, 7.4, and 8 for ***o*-** and ***m*-BCDs**. On the other hand, ***p*-BCDs** exhibited a small difference of fluorescence intensity at various pH. This is indicative of the pH-independent fluorescence chemosensor for ***p*-BCDs**. Consequently, the HEPES buffer pH 7.4 was chosen for sensing approach of this nanomaterial.

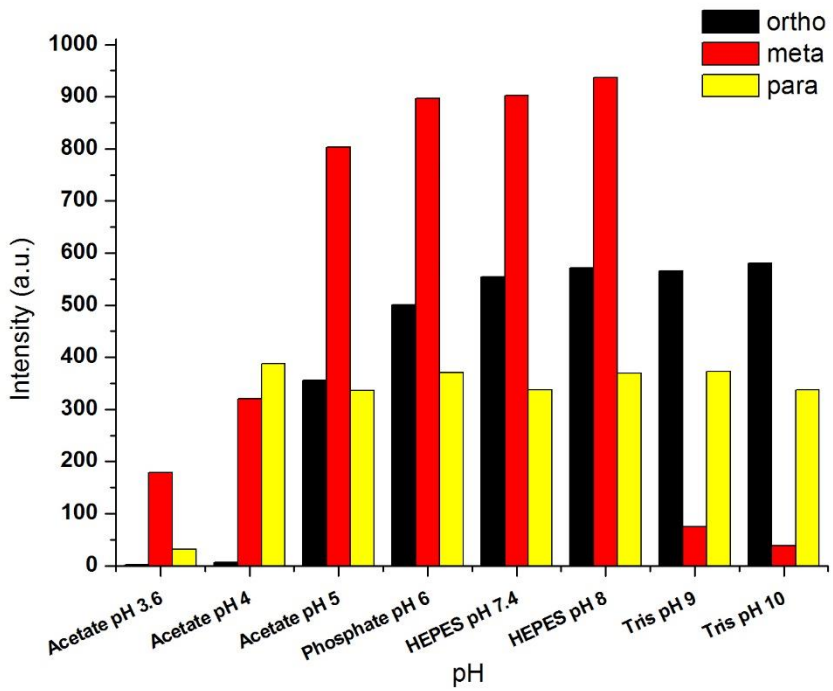

Figure 3.12 Determination of pH effect on three materials (***o*-BCDs**, ***m*-BCDs** and ***p*-BCDs**) with various pH in the range of 3.6-10.

3.4 The sensing properties of all BCDs towards H_2O_2

3.4.1 The studies on the reaction time between BCDs and H_2O_2

To explore the reaction time of **BCDs** toward H_2O_2, the fluorescence responses at various times from 0 to 60 min were carried out in HEPES buffer pH 7.4. The fluorescence spectra of ***o*-** and ***p*-BCDs** demonstrated a small fluorescent change in the presence of 10 mM H_2O_2 as shown in the figure 3.13a and 3.13c. On the contrary, the gradual florescence quenching of ***m*-BCDs** after adding 0.5 mM H_2O_2 at different time was observed in figure 3.13b. Increase of fluorescence quenching of ***m*-BCDs** corresponded to the increase of time, especially, the complete quenching of emission band demonstrated at 60 min. These results were possibly caused that boronic acid (B-OH) doped **BCDs** was easily oxidized to hydroxyl group. Therefore, the change of fluorescence intensity for ***m*-BCDs** towards H_2O_2 depends on the reaction time except for ***o*-BCDs** and ***p*-BCDs** whose structures did not contain the B-OH site on the edge of graphene sheet. The reaction time between **BCDs** and H_2O_2 was chosen at 15 minutes for further studies because this time is a short time period to provide the obviously fluorescence changes of all **BCDs**.

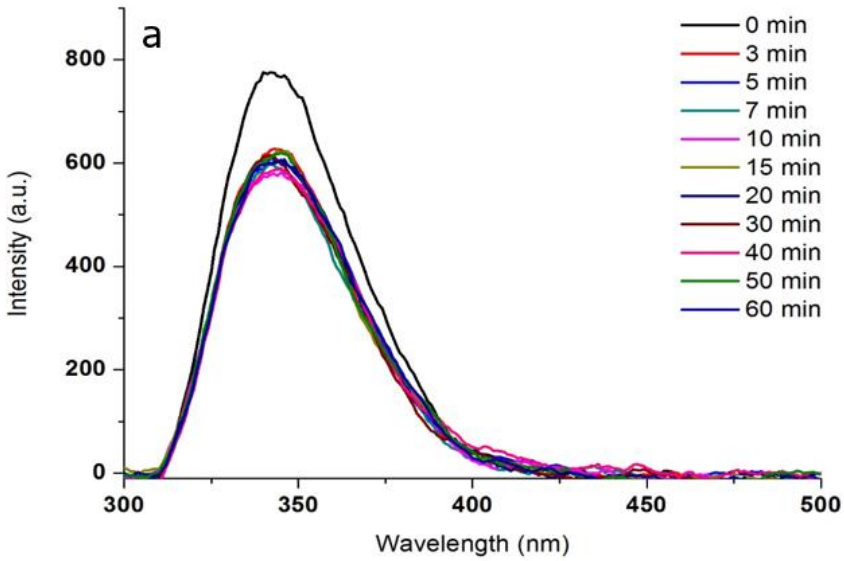

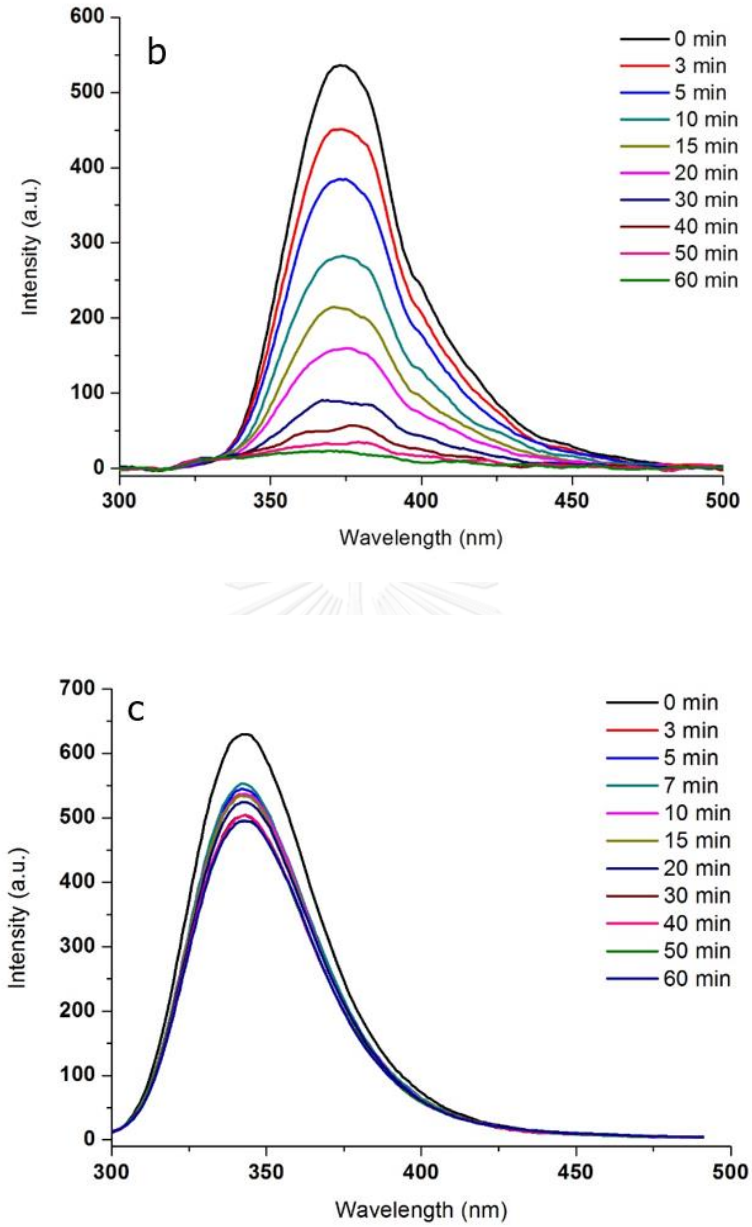

Figure 3.13 Fluorescence spectra of ***o*-BCDs** (a), ***m*-BCDs** (b) and ***p*-BCDs** (c) with various times (0-60 min) after addition of H_2O_2 (10 mM for o-**BCDs** and p-**BCDs** and 1 mM for ***m*-BCDs**).

3.4.2 The studies on the interaction between BCDs and H_2O_2 by fluorescence titration

In this study, the fluorescence spectra of ***o*-BCDs**, ***m*-BCDs** and ***p*-BCDs** toward various H_2O_2 concentration were displayed in figure 4.14-4.16. The fluorescence bands at 345, 375 and 343 nm for ***o*-BCDs**, ***m*-BCDs** and ***p*-BCDs**, respectively, were gradually quenched upon the increment of H_2O_2 concentration. The H_2O_2 possibly converted the C-B-OH bond to be hydroxyl group based on **BCDs** resulting in fluorescence quenching of **BCDs**. These results suggested that boronic acid on the edge of ***m*-BCDs** easily reacted with H_2O_2 compared to B-O bond in ***o*-BCDs** and ***p*-BCDs**. The limit of detection (LOD) of all **BCDs** toward H_2O_2 calculated by the equation 4 was 7.17, 0.026 and 17.53 mM under linear range of 10-59, 0.1-1 and 10-75 mM for ***o*-BCDs**, ***m*-BCDs** and ***p*-BCDs**, respectively (Figure 3.14-3.16). Surprisingly, the concentration of H_2O_2 to oxidize ***o*-BCDs** and ***p*-BCDs** was much higher than that of H_2O_2 for ***m*-BCDs**.

$$\text{LOD} = \frac{3\text{SD}}{\text{Slope}} \qquad (4)$$

$$\text{LOQ} = \frac{10\text{SD}}{\text{Slope}} \qquad (5)$$

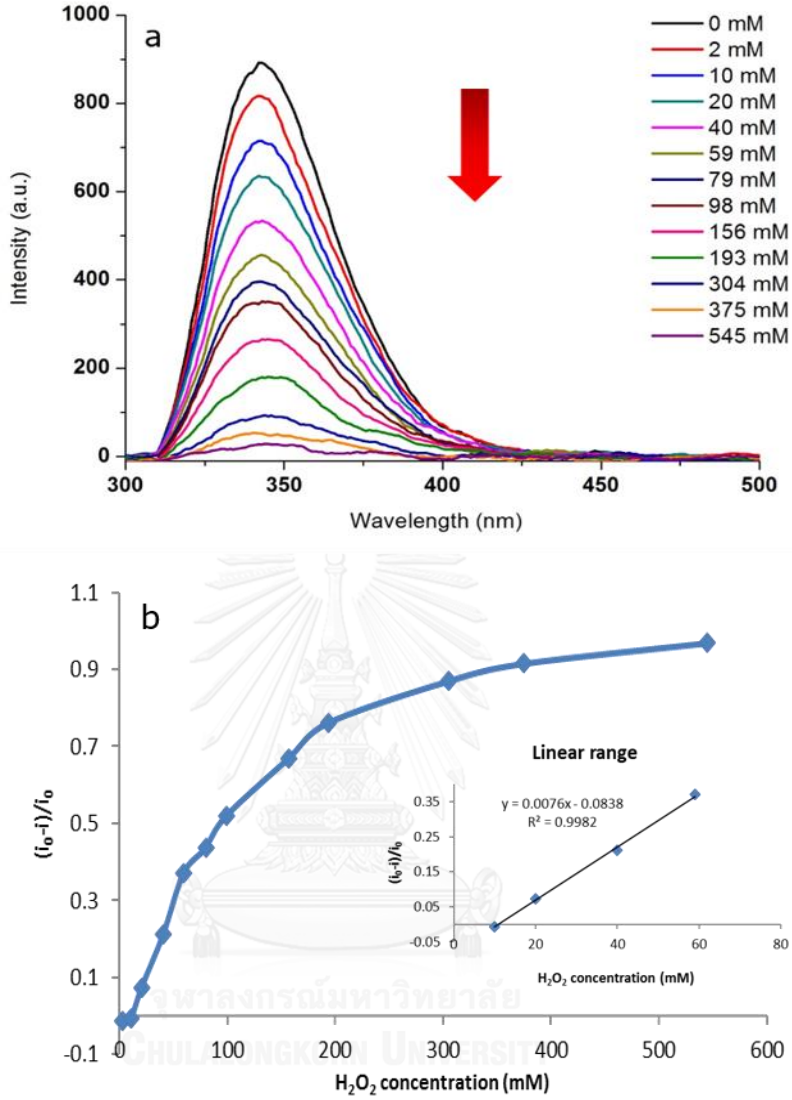

Figure 3.14 The fluorescence spectral changes of ***o*-BCDs** (a), and the quenching efficiency $(I_0-I)/I_0$ of ***o*-BCDs** after addition of H_2O_2 (0-700 mM), where I_0 and I are fluorescence intensity of ***o*-BCDs** in the presence and absence of H_2O_2, respectively. Inset: the linear range of H_2O_2 detection (10-59 mM).

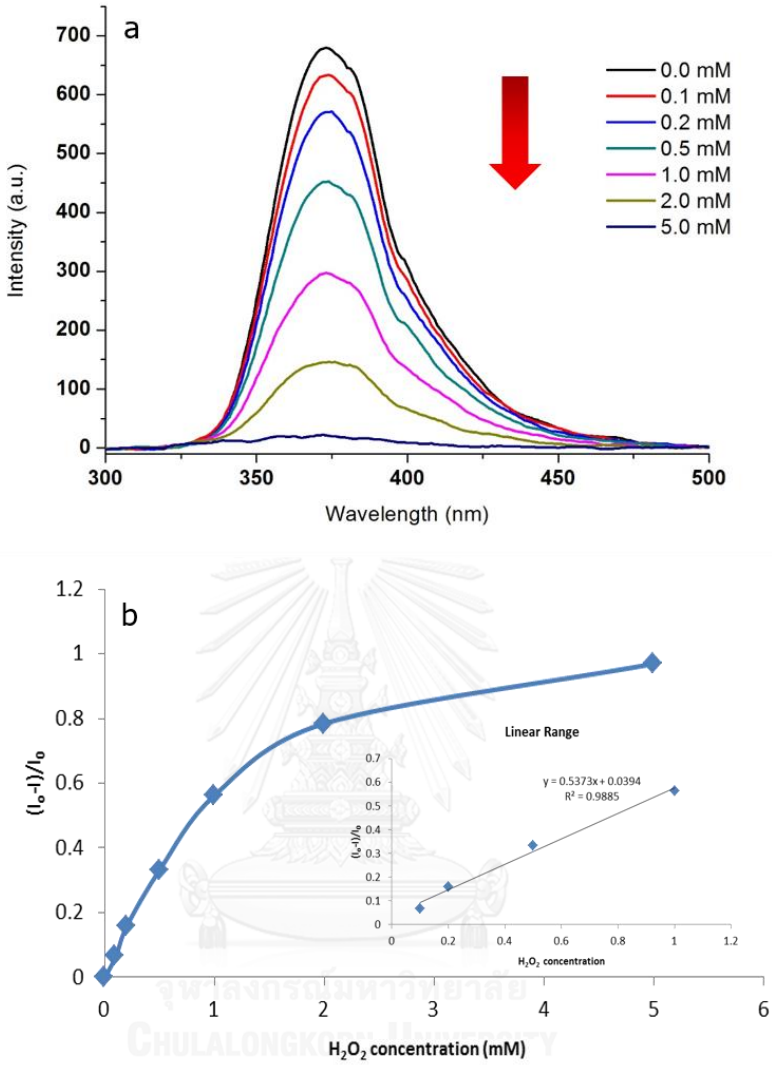

Figure 3.15 The fluorescence spectral changes of ***m*-BCDs** (a), and (b) the quenching efficiency $(I_0-I)/I_0$ of ***m*-BCDs** after addition of H_2O_2 (0-5 mM), where I_0 and I are fluorescence intensity of ***m*-BCDs** in the presence and absence of H_2O_2, respectively. Inset: the linear range of H_2O_2 titration (0.1-1 mM).

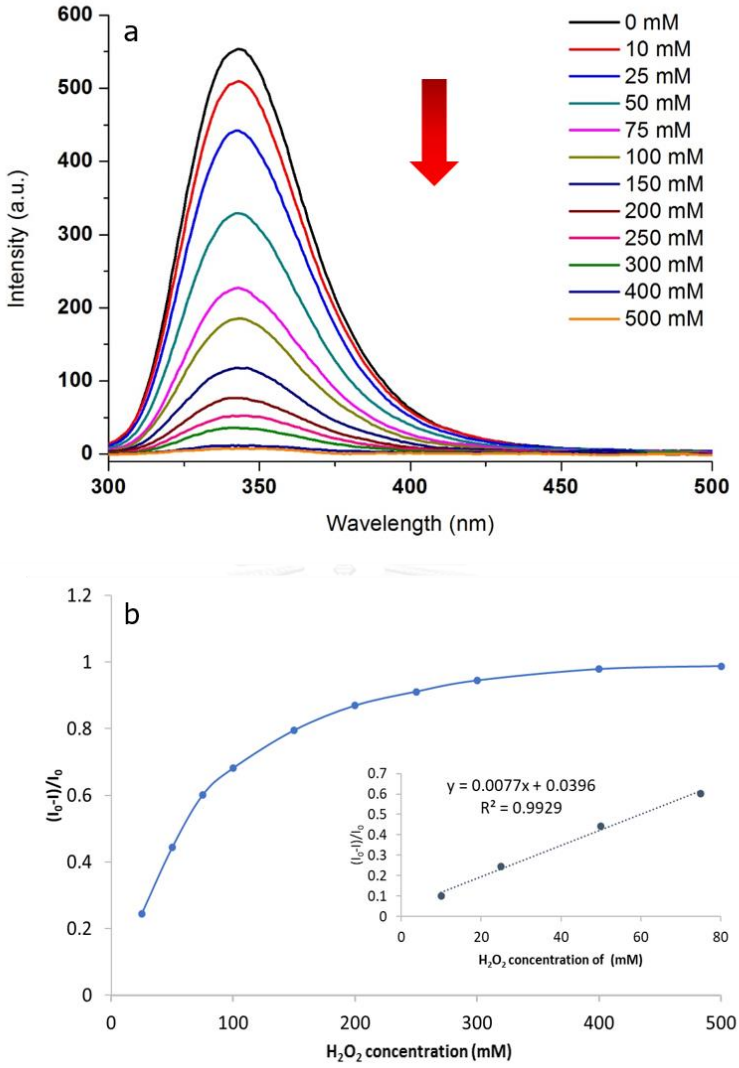

Figure 3.16 The fluorescence spectral changes of ***p*-BCDs** (a), and (b) the quenching efficiency $(I_0\text{-}I)/I_0$ of ***p*-BCDs** after addition of H_2O_2 (0-500 mM), where I_0 and I are fluorescence intensity of ***p*-BCDs** in the presence and absence of H_2O_2, respectively. Inset: the linear range of H_2O_2 detection (10-75 mM).

Extensive work for visual determination of **BCDs** and H_2O_2 was examined under UV light. The solution of **BCDs** exhibited the strong blue brightness under UV light at λ_{ex} 365 nm. Upon the reaction of **BCDs** and H_2O_2, the blue brightness of each solution was quenched as show in figure 3.17.

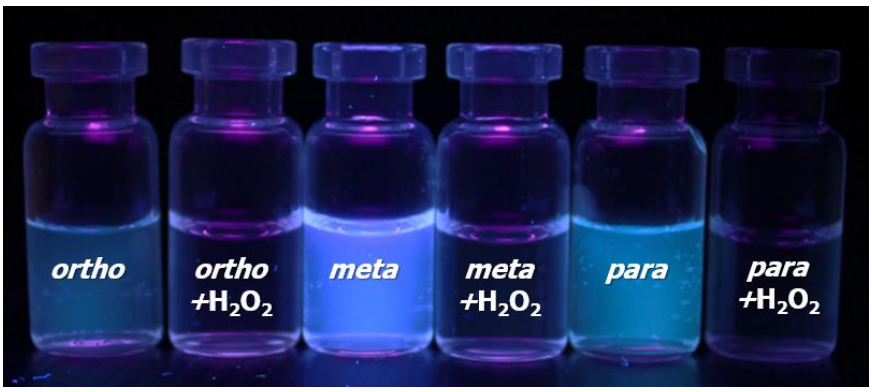

Figure 3.17 The solutions of each **BCDs** (***o*-BCDs**, ***m*-BCDs** and ***p*-BCDs** at approximately 14 mg/mL) under UV irradiation with the absence (left) and presence (right) of H_2O_2 at 6 M.

3.4.3 Fluorescent sensing of BCDs towards glucose via enzymatic reaction

3.4.3.1 Design concept of enzymatic reaction

Based on the basic knowledge of enzymatic reaction of GOx, the specific reaction between glucose and GOx with boronic based chemosensor was illustrated in Scheme 3.2 [16].

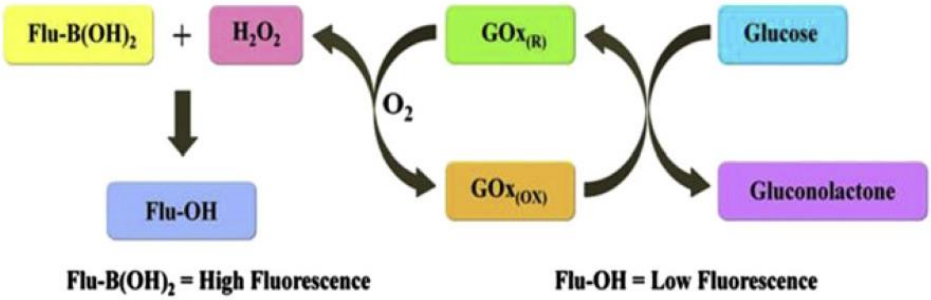

Scheme 3.2 The GOx enzymatic mechanism for detection of glucose using boronic derivative as fluorescence sensor [16].

The enzyme GOx was wildly used in biomedical application to determine the glucose levels in biological system. The reaction of glucose and GOx in the presence of O_2 will actually produce gluconolactone and H_2O_2. Interestingly, the H_2O_2 acting as the oxidizing agent could completely oxidize boronic acid group based on the fluorescence probe via hydroboration reaction to produce the hydroxyl group (OH) in

fluorescence probe leading the fluorescent change. This aspect was expected to determine the amount of glucose in the biological system

3.4.3.2 The glucose sensing properties of BCDs by enzymatic reaction of GOx

Due to the fact that boronic acid can bind with *cis*-diol of saccharide [34], the chemical structures of saccharide especially glucose and fructose have *cis*-diol position as shown in figure 3.18. According to a large fluorescence quenching of ***m*-BCDs** upon the addition of H_2O_2, the ***m*-BCDs** was candidate for studying the glucose sensing via enzymatic reaction. As the characterization by XPS and ^{11}B-NMR, we found that **BCDs** contained boronic acid group which normally preferred to bind with *cis*-diol of glucose and fructose. Therefore, the binding ability of ***m*-BCDs** towards glucose and fructose was firstly examined in HEPES buffer pH7.4. As seen the figure 3.19, the fluorescence intensity of ***m*-BCDs** at 375 nm was remained unchanged upon adding the glucose and fructose. It implied that the boronic acid on the edge of ***m*-BCDs** cannot bind to both saccharides causing the unchange of fluorescence response. Due to no direct interaction between glucose and ***m*-BCDs** leading to no interference signal from self-interaction, this is a benefit material in glucose sensing via enzymatic reaction.

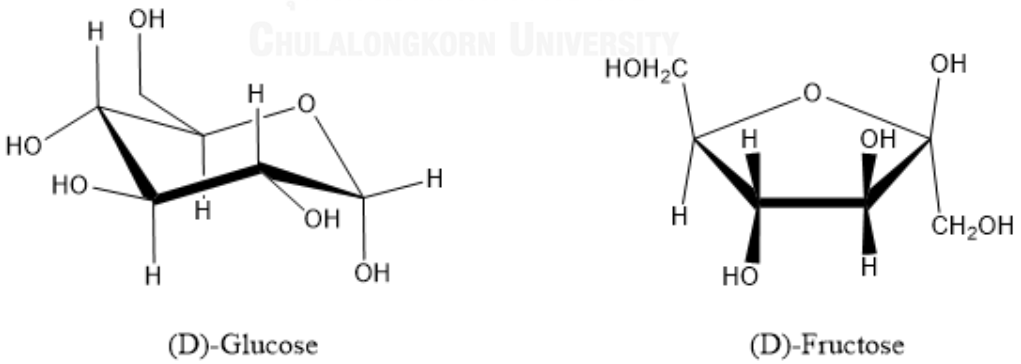

Figure 3.18 The chemical structures of glucose (left) and fructose (right).

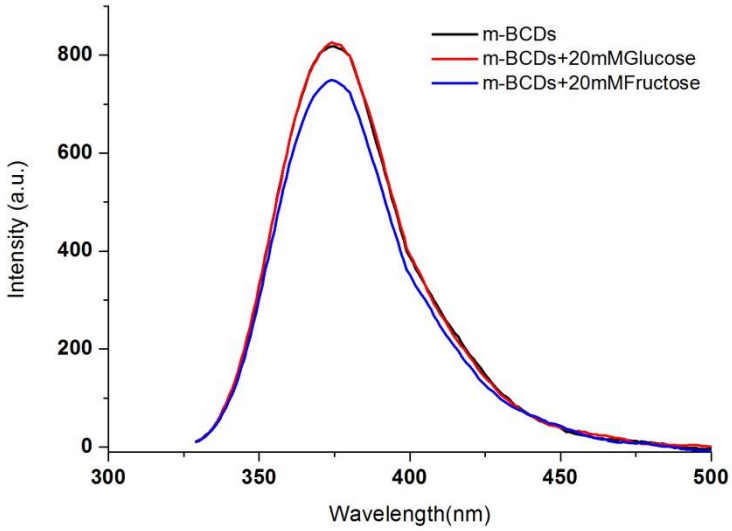

Figure 3.19 The fluorescence spectral changes of ***m*-BCDs** in the presence of 20 mM glucose and fructose in HEPES buffer pH 7.4 under excitation wavelength at 310 nm.

To confirm the specific reaction of GOx and glucose, the reaction between ***m*-BCDs** and 20 mM monosaccharides (glucose or fructose) and 1 unit of GOx was carried out by fluorescence spectroscopy. In the case of glucose addition, the fluorescence signal of ***m*-BCDs** was significantly changed upon the addition of GOx for 60 min under O_2 condition (Figure 3.20). On the other hand, the fluorescence intensity of ***m*-BCDs** remained unchanged in the case of fructose at the same condition. The glucose was completely transformed to gluconic acid and H_2O_2 which enabled to oxidize B-OH based ***m*-BCDs** to hydroxy group resulting in the fluorescence quenching under PET process. The result revealed that the GOx was an important enzyme for specific reaction with glucose.

Figure 3.20 Determination of fluorescence responses of ***m*-BCDs** at 375 nm with glucose and fructose before and after adding glucose oxidase (black bar and red bar, respectively) in HEPES buffer pH 7.4.

3.4.3.3 The studies on the effect of unit of glucose oxidase

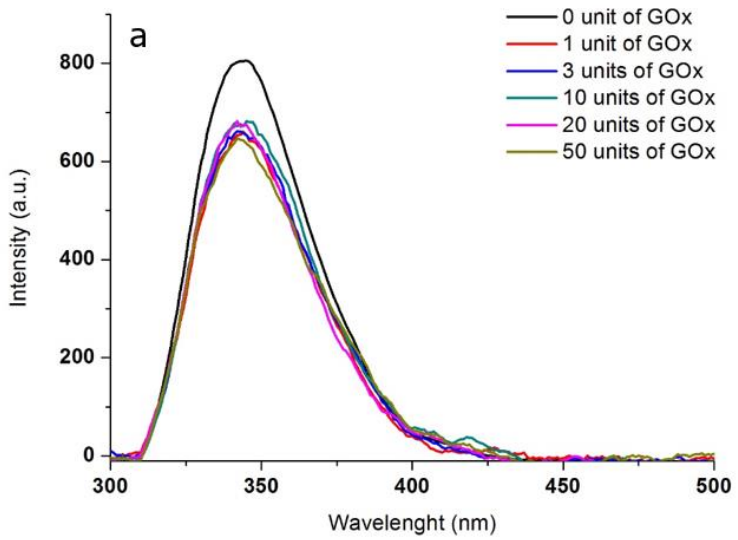

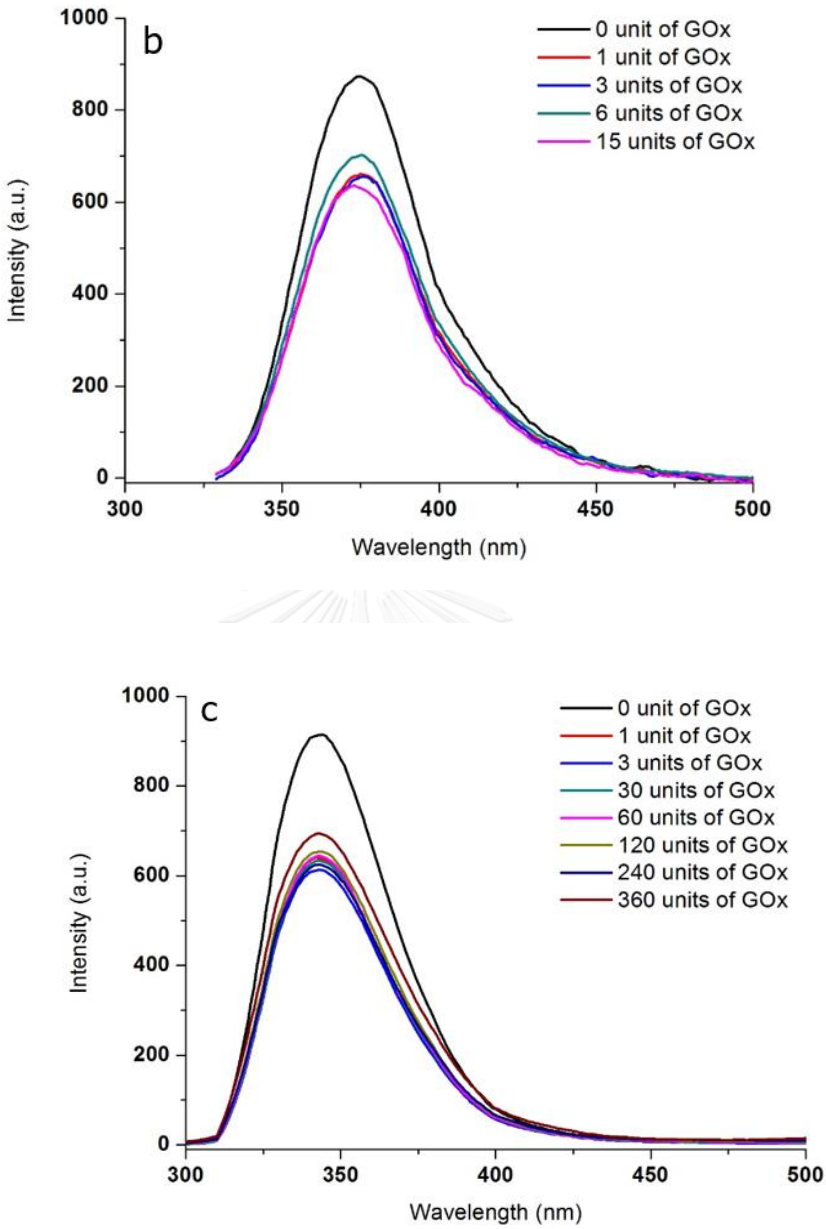

Figure 3.21 Fluorescence spectra of ***o*-BCDs** (a), ***m*-BCDs** (b) and ***p*-BCDs** (c) with various unit of glucose oxidase. (0-50, 0-15, 0-360 units for ***o*-BCDs**, ***m*-BCDs** and ***p*-BCDs**, respectively).

Under enzymatic reaction, the amount of GOx is an important factor for sensing purpose of **BCDs** and glucose. Figure 3.21 exhibited the fluorescence responses of all

BCDs by varying the unit of GOx in the presence of 10 mM glucose for ***o*-BCDs** and ***p*-BCDs** and 1 mM glucose for ***m*-BCDs**. The results showed that the fluorescence signals of all **BCDs** slightly changed with increasing the amount of glucose oxidase (GOx). As a result, we expected that only 1 unit of GOx reacted completely with glucose to generate hydrogen peroxide in the presence of O_2 at 37°C. It was proposed that the fluorescence changes of **BCDs** depended on the concentration of H_2O_2 which was generated from enzymatic reaction of glucose and GOx. In order to further study the glucose sensing properties of **BCDs**, the suitable amount of GOx at 1 unit was applied for all enzymatic reaction experiments.

3.4.3.4 The studies on the reaction time of enzymatic system

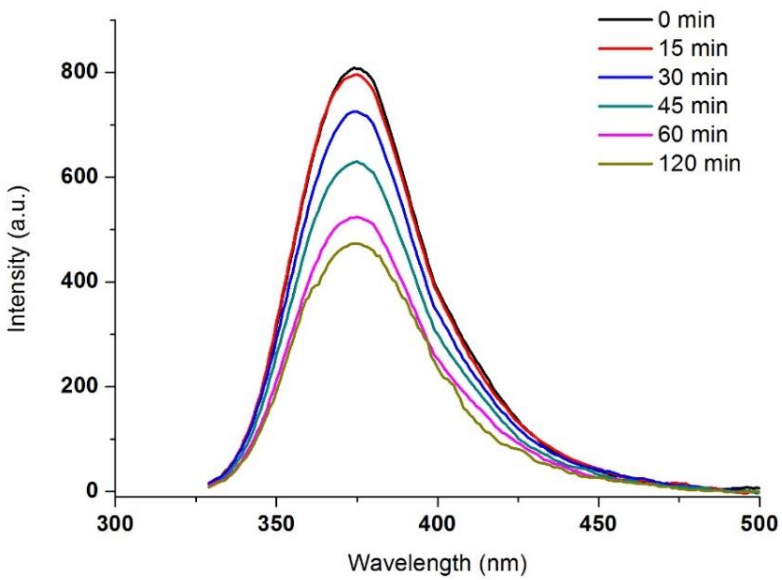

Figure 3.22 The fluorescence spectral changes of ***m*-BCDs** at different reaction time (0-60 mins) under excitation wavelength at 310 nm in HEPES buffer pH 7.4.

To verify the reaction time, the ***m*-BCDs** were a representative material for studying on a reaction time in the enzymatic process. The fluorescence intensity at 375 nm of ***m*-BCDs** was conducted under excitation wavelength of 310 nm. The reaction time of enzymatic reaction was investigated from 0 to 120 min in the presence of 1 unit GOx and 1 mM glucose. The fluorescence intensity of ***m*-BCDs** was gradually decreased as a function of the reaction time (Figure 3.22). The results indicated that

the amount of H_2O_2 generated by interaction between GOx and glucose depended on the reaction time. However, the enzymatic reaction time of **BCDs** materials toward 1 mM glucose was selected at 60 min which showed a large change of fluorescence spectrum and the proper reaction time for real-time detection in the sensing application.

3.4.3.5 The fluorescence titration studies of BCDs and glucose via enzymatic reaction

The fluorescence titration of each **BCDs** has been examined under enzymatic reaction of GOx and the different concentration of glucose in HEPES buffer pH 7.4. The fluorescence responses of ***o*-BCDs**, ***m*-BCDs** and ***p*-BCDs** were monitored at 345, 375 and 343 nm, respectively (Figure 3.23). Interestingly, the florescence intensity of ***m*-BCDs** was gradually quenched upon the increment amount of glucose and the complete quenching was observed at 20 mM glucose. On the other hand, ***o*-** and ***p*-BCDs** showed a small quenching of emission bands at 345 nm and 343 nm, respectively. The results indicated that, in comparison of fluorescence quenching of emission bands at the concentration of glucose at 20 mM, the quenching tendency of each material is in order of ***m*-BCDs** >> ***o*-BCDs** > ***p*-BCDs**. Considering, the fluorescence titration curve of ***m*-BCDs** toward glucose in the presence of GOx exhibited the propational changes regarding to the increment of glucose. Therefore, the calibration curve of ***m*-BCDs** and glucose can be used to find the limit of detection (LOD) and limit of quantitation (LOQ) in the range of 2 mM–15 mM (Figure 3.24). The LOD and LOQ calculated by the equation 3 and 4 were 0.857 mM and 2.858 mM, respectively. Particular of ***m*-BCDs** highlights as a promising selectivity and sensitivity for detection of glucose via enzymatic GOx reaction.

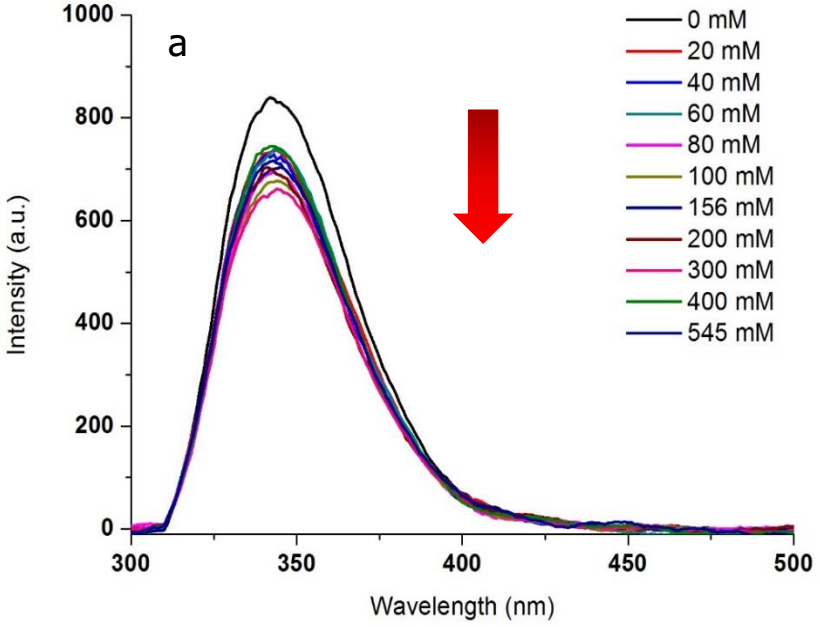
a
Intensity (a.u.)
Wavelength (nm)
0 mM
20 mM
40 mM
60 mM
80 mM
100 mM
156 mM
200 mM
300 mM
400 mM
545 mM

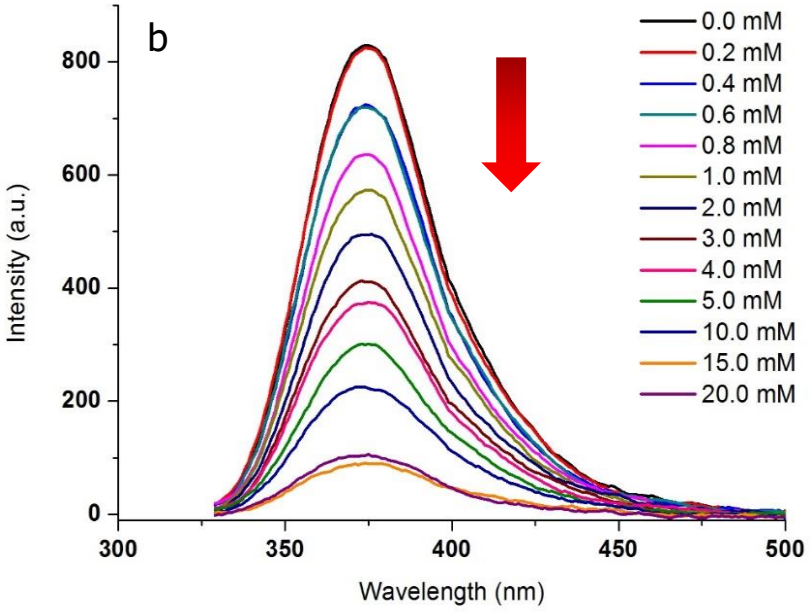
b
Intensity (a.u.)
Wavelength (nm)
0.0 mM
0.2 mM
0.4 mM
0.6 mM
0.8 mM
1.0 mM
2.0 mM
3.0 mM
4.0 mM
5.0 mM
10.0 mM
15.0 mM
20.0 mM

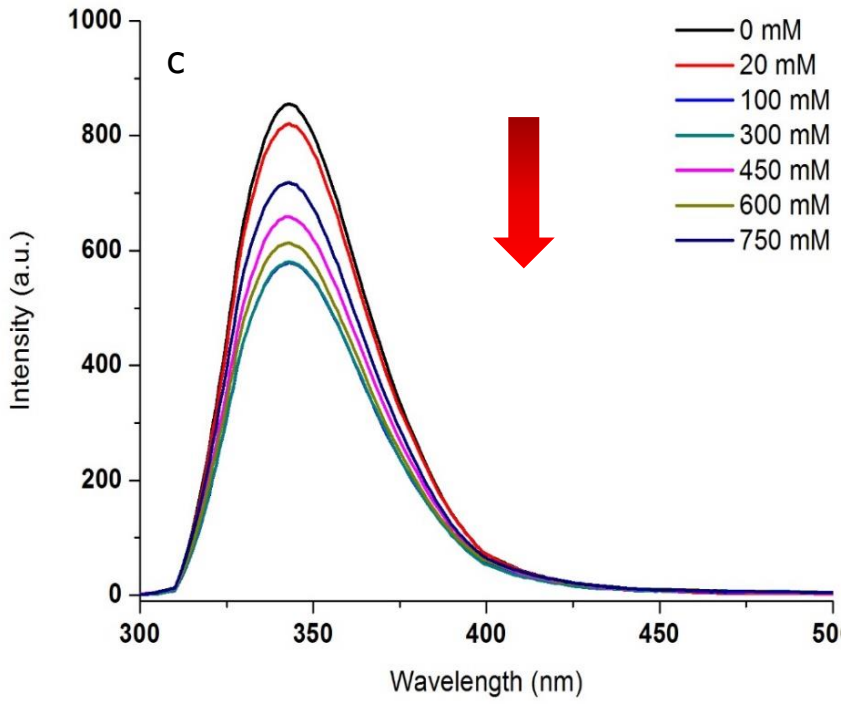

Figure 3.23 The fluorescence titration spectral of ***o*-BCDs** (a), ***m*-BCDs** (b) and ***p*-BCDs** (c) in the presence of various concentration of glucose (0-545, 0-20, 0-750 mM for ***o*-BCDs**, ***m*-BCDs** and ***p*-BCDs**, respectively.

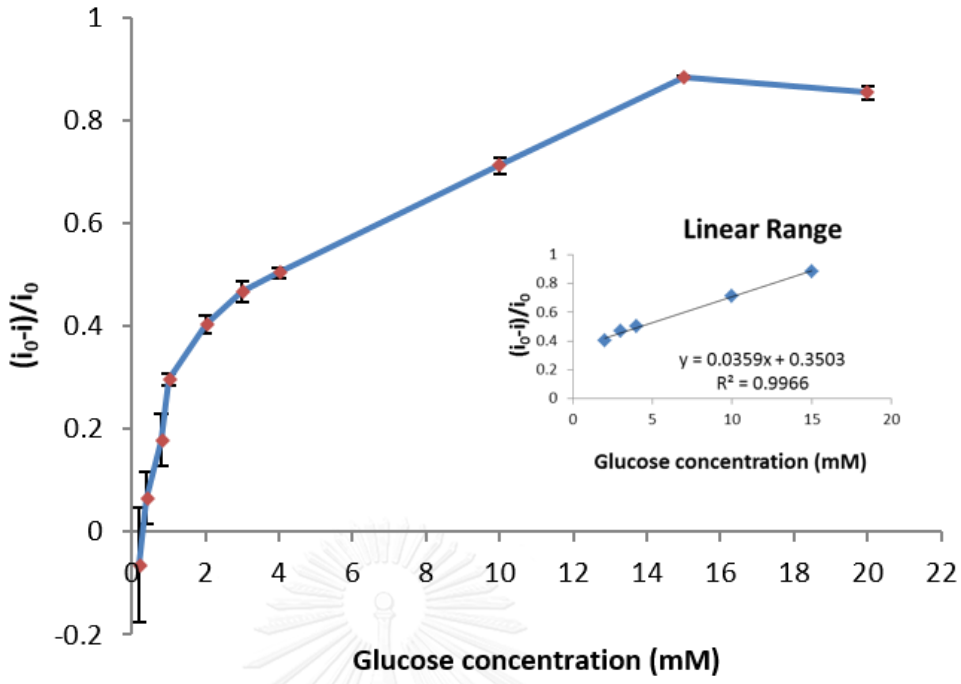

Figure 3.24 The quenching efficiency $(I_0-I)/I_0$ of ***m*-BCDs** after addition of glucose (0-20 mM) though enzymatic reaction, where I_0 and I are fluorescence intensity of ***m*-BCDs** in the presence and absence of glucose, respectively. Inset: the linear range of glucose detection.

CHAPTER IV
CONCLUSION

In this work, we have successfully synthesized the new fluorescence sensor based on B/N doped carbon dots by one step hydrothermal carbonization, namely ***o*-BCDs**, ***m*-BCDs** and ***p*-BCDs**, for glucose sensing. As the results of TEM images, it illustrated the ***o*-BCDs** and ***p*-BCDs** showing fairly uniform nanoparticles with an average particle size of 8 nm and 9 nm, respectively while ***m*-BCDs** have the varied particle sizes from 9-12 nm. From AFM images, it showed a single layer of graphene sheet of these materials. Furthermore, XPS techniques and ^{11}B-NMR spectroscopy were investigated to verify the component structure of **BCDs**. It was found that the component structure of ***o*-BCDs** and ***p*-BCDs** consists of the B-O group of B_2O_3, whereas structure of ***m*-BCDs** contained the boronic acid group (B-OH) on the edge of graphene sheet. All **BCDs** comprised the nitrogen atom doped in the structure in form of primary and quaternary amine. As these result, we hypothesized that the different isomer of starting material leads to the different structure of **BCDs** possibly caused by the electronic effect of NH_2 on the APBA.

For the photophysical properties, the **BCDs** (***o*-**, ***m*-** and ***p*-BCDs**) showed a strong excitation-independent fluorescent emission band at 345 nm, 375 nm and 343 nm, respectively, in HEPES buffer pH 7.4. The quantum yield of ***o*-BCDs**, ***m*-BCDs** and ***p*-BCDs** was 3.02%, 17.26% and 3.30%, respectively. The quantum yield of ***m*-BCDs** was higher than the others which corresponded to the different structure of each **BCDs**. In addition, the studies on the fluorescence titration of **BCDs** towards H_2O_2 exhibited the gradual decrease of emission bands at 345 nm, 375 nm and 343 nm for ***o*-BCDs**, ***m*-BCDs** and ***p*-BCDs**, respectively**.** Interestingly, the ***m*-BCDs** showed a great quenching compared to ***o*-BCDs** and ***p*-BCDs**. The detection limit of ***o*-BCDs**, ***m*-BCDs** and ***p*-BCDs** toward H_2O_2 was 7.17 mM, 0.026 mM and 17.53 mM, respectively. According to the sensing properties of ***m*-BCDs** and glucose via enzymatic reaction, the ***m*-BCDs** exhibited gradually the fluorescence quenching at 375 nm corresponding to the increment of glucose. The limit of detection (LOD) and the limit of quantitative

(LOQ) of ***m*-BCDs** in glucose detection was 0.857 mM and 2.858 mM, respectively, which was in the range of diabetes diagnosis. On the other hand, ***o*-** and ***p*-BCDs** did not perform the fluorescent changes regarding to the amount of glucose. As anticipated, the different substitution of B and N atom based starting materials would resulted in the different N/B species in these materials inducing the different photophysical properties and sensing affinity. Finally, we expected these new materials can be applied for applications of environmental monitoring and clinical diagnosis.

REFERENCES

[1] Bankar, S.B., Bule, M.V., Singhal, R.S., and Ananthanarayan, L. Glucose oxidase — An overview. Biotechnology Advances 27(4) (2009): 489-501.

[2] Diseases, N. N. I. o. D. a. D. a. K. Diabetes Complications [Online]. 2016. Available from: https://medlineplus.gov/diabetescomplications.html [June 27]

[3] Zhu, S., Song, Y., Zhao, X., Shao, J., Zhang, J., and Yang, B. The photoluminescence mechanism in carbon dots (graphene quantum dots, carbon nanodots, and polymer dots): current state and future perspective. Nano Research 8(2) (2015): 355-381.

[4] Li, Y.-H., Zhang, L., Huang, J., Liang, R.-P., and Qiu, J.-D. Fluorescent graphene quantum dots with a boronic acid appended bipyridinium salt to sense monosaccharides in aqueous solution. Chemical Communications 49(45) (2013): 5180-5182.

[5] Clark, L.C. and Lyons, C. ELECTRODE SYSTEMS FOR CONTINUOUS MONITORING IN CARDIOVASCULAR SURGERY. Annals of the New York Academy of Sciences 102(1) (1962): 29-45.

[6] Long, F., Zhu, A., Gu, C., and Shi, H. Recent Progress in Optical Biosensors for Environmental Applications. (2013).

[7] Shankaran, D.R., Gobi, K.V., and Miura, N. Recent advancements in surface plasmon resonance immunosensors for detection of small molecules of biomedical, food and environmental interest. Sensors and Actuators B: Chemical 121(1) (2007): 158-177.

[8] Van Dorst, B., et al. Recent advances in recognition elements of food and environmental biosensors: A review. Biosensors and Bioelectronics 26(4) (2010): 1178-1194.

[9] Wanekaya, A.K., Chen, W., and Mulchandani, A. Recent biosensing developments in environmental security. Journal of Environmental Monitoring 10(6) (2008): 703-712.

[10] Borisov, S.M. and Wolfbeis, O.S. Optical Biosensors. Chemical Reviews 108(2) (2008): 423-461.

[11] Fan, X., White, I.M., Shopova, S.I., Zhu, H., Suter, J.D., and Sun, Y. Sensitive optical biosensors for unlabeled targets: a review. Anal Chim Acta 620(1-2) (2008): 8-26.

[12] Ligler, F.S. Perspective on optical biosensors and integrated sensor systems. Anal Chem 81(2) (2009): 519-26.

[13] Palchetti, I. and Mascini, M. Nucleic acid biosensors for environmental pollution monitoring. Analyst 133(7) (2008): 846-54.

[14] Mirón, J., González, M.P., Vázquez, J.A., Pastrana, L., and Murado, M.A. A mathematical model for glucose oxidase kinetics, including inhibitory, deactivant and diffusional effects, and their interactions. Enzyme and Microbial Technology 34(5) (2004): 513-522.

[15] Clay, J.M. and Vedejs, E. Hydroboration with Pyridine Borane at Room Temperature. Journal of the American Chemical Society 127(16) (2005): 5766-5767.

[16] Wannajuk, K., Jamkatoke, M., Tuntulani, T., and Tomapatanaget, B. Highly specific-glucose fluorescence sensing based on boronic anthraquinone derivatives via the GOx enzymatic reaction. Tetrahedron 68(43) (2012): 8899-8904.

[17] Sun, Y.-P., et al. Quantum-Sized Carbon Dots for Bright and Colorful Photoluminescence. Journal of the American Chemical Society 128(24) (2006): 7756-7757.

[18] Lim, S.Y., Shen, W., and Gao, Z. Carbon quantum dots and their applications. Chemical Society Reviews 44(1) (2015): 362-381.

[19] Song, Y., Zhu, S., and Yang, B. Bioimaging based on fluorescent carbon dots. RSC Advances 4(52) (2014): 27184-27200.

[20] Zheng, X.T., Ananthanarayanan, A., Luo, K.Q., and Chen, P. Glowing graphene quantum dots and carbon dots: properties, syntheses, and biological applications. Small 11(14) (2015): 1620-36.

[21] Peng, J., et al. Graphene Quantum Dots Derived from Carbon Fibers. Nano Letters 12(2) (2012): 844-849.

[22] Tao, H., et al. In Vivo NIR Fluorescence Imaging, Biodistribution, and Toxicology of Photoluminescent Carbon Dots Produced from Carbon Nanotubes and Graphite. Small 8(2) (2012): 281-290.

[23] Shen, J., Zhu, Y., Yang, X., and Li, C. Graphene quantum dots: emergent nanolights for bioimaging, sensors, catalysis and photovoltaic devices. Chemical Communications 48(31) (2012): 3686-3699.

[24] Xu, H., Zhou, S., Xiao, L., Wang, H., Li, S., and Yuan, Q. Fabrication of a nitrogen-doped graphene quantum dot from MOF-derived porous carbon and its application for highly selective fluorescence detection of Fe3+. Journal of Materials Chemistry C 3(2) (2015): 291-297.

[25] Jin, S.H., Kim, D.H., Jun, G.H., Hong, S.H., and Jeon, S. Tuning the Photoluminescence of Graphene Quantum Dots through the Charge Transfer Effect of Functional Groups. ACS Nano 7(2) (2013): 1239-1245.

[26] Tian, T., He, Y., Ge, Y., and Song, G. One-pot synthesis of boron and nitrogen co-doped carbon dots as the fluorescence probe for dopamine based on the redox reaction between Cr(VI) and dopamine. Sensors and Actuators B: Chemical 240 (2017): 1265-1271.

[27] Qian, Z., Ma, J., Shan, X., Feng, H., Shao, L., and Chen, J. Highly Luminescent N-Doped Carbon Quantum Dots as an Effective Multifunctional Fluorescence Sensing Platform. Chemistry – A European Journal 20(8) (2014): 2254-2263.

[28] Jaiswal, A., Ghosh, S.S., and Chattopadhyay, A. One step synthesis of C-dots by microwave mediated caramelization of poly(ethylene glycol). Chemical Communications 48(3) (2012): 407-409.

[29] Yang, Y., et al. One-step synthesis of amino-functionalized fluorescent carbon nanoparticles by hydrothermal carbonization of chitosan. Chemical Communications 48(3) (2012): 380-382.

[30] Li, Y., et al. Nitrogen-doped graphene quantum dots with oxygen-rich functional groups. J Am Chem Soc 134(1) (2012): 15-8.

[31] Qu, Z.-b., et al. Boronic acid functionalized graphene quantum dots as a fluorescent probe for selective and sensitive glucose determination in microdialysate. Chemical Communications 49(84) (2013): 9830-9832.

[32] Shen, P. and Xia, Y. Synthesis-Modification Integration: One-Step Fabrication of Boronic Acid Functionalized Carbon Dots for Fluorescent Blood Sugar Sensing. Analytical Chemistry 86(11) (2014): 5323-5329.

[33] Shan, X., Chai, L., Ma, J., Qian, Z., Chen, J., and Feng, H. B-doped carbon quantum dots as a sensitive fluorescence probe for hydrogen peroxide and glucose detection. Analyst 139(10) (2014): 2322-2325.

[34] Zhang, L., Zhang, Z.-Y., Liang, R.-P., Li, Y.-H., and Qiu, J.-D. Boron-Doped Graphene Quantum Dots for Selective Glucose Sensing Based on the "Abnormal" Aggregation-Induced Photoluminescence Enhancement. Analytical Chemistry 86(9) (2014): 4423-4430.

[35] Jiang, K., et al. Red, Green, and Blue Luminescence by Carbon Dots: Full-Color Emission Tuning and Multicolor Cellular Imaging. Angewandte Chemie International Edition 54(18) (2015): 5360-5363.

[36] Rocha, S.N., Abrahão-Neto, J., Cerdán, M.E., González-Siso, M.I., and Gombert, A.K. Heterologous expression of glucose oxidase in the yeast Kluyveromyces marxianus. Microbial Cell Factories 9(1) (2010): 4.

[37] Shaw, J.E., Sicree, R.A., and Zimmet, P.Z. Global estimates of the prevalence of diabetes for 2010 and 2030. Diabetes Research and Clinical Practice 87(1) (2010): 4-14.

[38] Song, Y., Qu, K., Zhao, C., Ren, J., and Qu, X. Graphene Oxide: Intrinsic Peroxidase Catalytic Activity and Its Application to Glucose Detection. Advanced Materials 22(19) (2010): 2206-2210.

[39] Chen, H., Fang, A., He, L., Zhang, Y., and Yao, S. Sensitive fluorescent detection of H2O2 and glucose in human serum based on inner filter effect of squaric acid-iron(III) on the fluorescence of upconversion nanoparticle. Talanta 164 (2017): 580-587.

[40] Kumar, D., et al. Eu:Y2O3 highly dispersed fluorescent PVA film as turn off luminescent probe for enzyme free detection of H_2O_2. Sensors and Actuators B: Chemical 247 (2017): 170-178.

[41] Liu, Y., Li, H., Guo, B., Wei, L., Chen, B., and Zhang, Y. Gold nanoclusters as switch-off fluorescent probe for detection of uric acid based on the inner filter effect of hydrogen peroxide-mediated enlargement of gold nanoparticles. Biosensors and Bioelectronics 91 (2017): 734-740.

[42] Ding, Y., et al. A facile strategy for the preparation of ZnS nanoparticles deposited on montmorillonite and their higher catalytic activity for rapidly colorimetric detection of H2O2. Materials Science and Engineering: C 67 (2016): 188-194.

[43] Liu, Q., et al. One-step synthesis of uniform nanoparticles of porphyrin functionalized ceria with promising peroxidase mimetics for H2O2 and glucose colorimetric detection. Sensors and Actuators B: Chemical 240 (2017): 726-734.

[44] Ni, P., et al. Prussian blue nanocubes peroxidase mimetic-based colorimetric assay for screening acetylcholinesterase activity and its inhibitor. Sensors and Actuators B: Chemical 240 (2017): 1314-1320.

[45] ElKaoutit, M., Naranjo-Rodriguez, I., Domínguez, M., Hernández-Artiga, M.P., Bellido-Milla, D., and Hidalgo-Hidalgo de Cisneros, J.L. A third-generation hydrogen peroxide biosensor based on Horseradish Peroxidase (HRP) enzyme immobilized in a Nafion–Sonogel–Carbon composite. Electrochimica Acta 53(24) (2008): 7131-7137.

[46] Lu, J., et al. Electrochemiluminescence of blue-luminescent graphene quantum dots and its application in ultrasensitive aptasensor for adenosine triphosphate detection. Biosensors and Bioelectronics 47 (2013): 271-277.

[47] Mattarozzi, L., Cattarin, S., Comisso, N., Guerriero, P., Musiani, M., and Verlato, E. Preparation of porous nanostructured Ag electrodes for sensitive electrochemical detection of hydrogen peroxide. Electrochimica Acta 198 (2016): 296-303.

[48] Wang, Z.-X., et al. Synergistic contributions by decreasing overpotential and enhancing electrocatalytic reduction in ONPCNRs/SWCNTs nanocomposite for highly sensitive nonenzymatic detection of hydrogen peroxide. Sensors and Actuators B: Chemical 246 (2017): 726-733.

[49] Zhang, Y., et al. Graphene quantum dots/gold electrode and its application in living cell H2O2 detection. Nanoscale 5(5) (2013): 1816-1819.

[50] Galindo, B., et al. Effect of the number of layers of graphene on the electrical properties of TPU polymers. IOP Conference Series: Materials Science and Engineering 64(1) (2014): 012008.

VITA

General Biographical Information

Miss Angkhana Khachonwongwattana was born on September 12, 1991 in Chachoengsao, Thailand. She got a high school diploma from Benchamaracharungsarit School (Mathematics and Sciences Programme), Chachoengsao in 2009. From there on, she has obtained the scholarship from the Research Professional Development Project under Science Achievement Scholarship of Thailand (SAST), under office of the Higher Education Commission (OHEC), Ministry of Education Thailand since 2010 until 2014. And then, she graduated and received her Bachelor's degree of Science in Chemistry from Kasetsart University in 2014. Afterwards, she has pursued Master's degree at Chulalongkorn University and has become a member of supramolecular research unit and worked under supervision of Assistant Professor Dr. Boosayarat Tomapatanaget and Dr. Wipark Anutrasakda.

About this research

2017 Angkhana Khachonwongwattana, Wipark Anutrasakda, Boosayarat Tomapatanaget "Synthesis of new boronic acid functionalized graphene quantum dots (BGQDs) for H2O2 detection" Proceedings of Pure and Applied Chemistry International Conference 2017, Centra Government Complex Hotel & Convention Centre Chaeng Watthana, Bangkok, Thailand, February 2-3, 2017, pp 728-731.

2016 Poster presentation at the 3rd International Congress on Advanced Materials (AM 2016), 27-30 November 2016, Centara Grand at Central Plaza Ladprao, Bangkok, Thailand.